*8th Mueller lecture presented at the 14th ISRM Congress, Brazil, CRC Press, pp. 141-182 in e-book*
*Pre-publication copy – personal copyright protected copy –*

# From common to best practices in underground rock engineering

P.K. Kaiser
*Professor Emeritus, Laurentian University and*
*President, GeoK Inc., Sudbury, Ontario, Canada*
pkaiser@laurentian.ca

ABSTRACT: Common practices are not necessarily best practices when judged from an economic or workplace safety perspective. As in other engineering disciplines, it is necessary to systematically improve engineering design practices. This lecture addresses some deficiencies in common practice that may lead to flawed or ineffective rock engineering solutions. More than ever, as we go deeper in underground construction, are rock engineers challenged by a number of opportunities that exist for improvements. In the past, common practices that worked well at shallow depth may need to be replaced as the rock mass behavior has changed and poses new hazards at depth. This lecture focuses specifically on opportunities resulting from better means to assess the vulnerability of excavations, to characterize the rock mass, for ground control, and rockburst damage mitigation. Theoretical considerations and field observations are used to justify the proposed changes and highlight practical implications and benefits. In the spirit of Prof. L. Müller, this lecture aims at pointing the way to future improvements in rock engineering, i.e. 'im Felsbau', and offers guidance on how to move from common to best practices.

It is an honor to present the 8th Müller lecture in memory of Prof. Leopold Müller and his achievements as the enthusiastic founder and first President of the ISRM in 1962. Today, we are remembering a man, whose vision moved rock engineering to a new science that influences geomechanics engineers all over the world. By creating the Society, he aimed at aggregating scientists interested in a new-born branch of science, rock mechanics, with the purpose of bringing together the scattered knowledge obtained by groups working more or less in isolation.

I like to start by acknowledging that many of my achievements, as well as the content of my presentation today, must be attributed to long-term collaborations with academic and industrial colleagues and also to many students whose careers have started in rock mechanics research. My mentors have taught me to question the status quo and to advance the state-of-the-art, and I like to dedicate this lecture to my most influential mentors Drs. N. Morgenstern, E. Hoek, E.T. Brown (6th ISRM President), and also to my wife Kathi, who has always supported my journey of discovery[1].

## 1 THE STORYLINE

Müller (1963), in the preamble to 'Der Felsbau', stated "Der Felsbau ist auf dem Wege, eine wissenschaftliche Disziplin zu werden. (Construction in rock ... is on the way to become a scientific discipline.)" Over the last 50+ years, the science of rock mechanics and its implementation through rock engineering has evolved into a mature discipline, and new challenges emerge as we tackle larger and deeper excavations in civil construction and mining.

He elaborated "Mit der Größe von Projekten wuchs die Verantwortung des Ingenieurs und des Baugeologen ganz bedeutend und zwang dazu, die bis anhin geübte gefühlsmäßige Behandlung dieser Aufgabe mehr und mehr zu verlassen und eine Theorie des Felsbaues zu erarbeiten." (With the size of projects, the responsibility of the engineer and the construction geologist grew quite significantly and forced us to leave intuitive treatment practices behind to develop a theory of rock engineering). In the

[1] https://videostream.laurentian.ca/Mediasite/Play/bf2879ebbe874213b42762775d593bc11d

spirit of his vision, it follows that rock engineering evolves over time and common practices need to be questioned and improved to arrive at best practices that lead to safer and more economic solutions.

Prof. Müller also suggested that it is sometimes necessary to go back to fundamentals to identify deficiencies in order to pave the road for progress.

Enormous progress has been made over the last decades and the new knowledge has found application through engineering standards, 'ISRM suggested methods', or common engineering practices. This is also reflected in the recent change of ISRM's name to 'International Society of Rock Mechanics and Rock Engineering'. Today, as in 1963, new challenges force us to leave our comfort zone of common practices and develop more sophisticated and, at the same time, simple, more efficient and effective rock engineering practices.

"Everything should be made as simple as possible, but not simpler" (attributed to A. Einstein). Common practices are often too simple and have frequently led to failures and costly mistakes, largely because the fundamental understanding of rock behavior and response to construction or mining are not fully reflected in experience-based approaches. Best practices make it simple, reflecting all essential or dominant Engineering Design Parameters (EDPs) – no more, no less. This means that unnecessary complexities have to be eliminated and representative rock engineering approaches adopted.

During the MTS lecture at the 50th US Rock Mechanics Symposium in 2016 on 'Underground rock engineering to match the rock's behavior – Challenges of managing highly stressed ground in civil and mining projects', the author suggested that dichotomies exist and gaps between reality and current practices have to be closed by the application of recent advances in rock mechanics research to arrive at sound rock engineering solutions.

"A robust rock engineering solution in underground mining or construction must respect the complexity and variability of the geology, consider the practicality and efficiency of construction, and provide safe and effective rock support. For this purpose, it is essential to anticipate the rock mass and excavation behavior early in the design process, i.e. at the tender stage before excavation techniques are chosen and designs are locked-in in construction contracts. Whereas it is possible in most engineering disciplines to select the most appropriate material for a given engineering problem, *in rock engineering, a design must be made to fit the rock, not vice versa.*

Lessons learned from excavation failures (Fig.1a) tell us that stressed rock at depth is less forgiving and that advances in rock mechanics demand a sound comprehension of the behavior of stress-damaged rock near excavations. Comprehension in this context means explaining all observations such that fiction can be separated from reality and engineering models and methods become congruent with the actual behavior of a rock mass." (Kaiser 2016b).

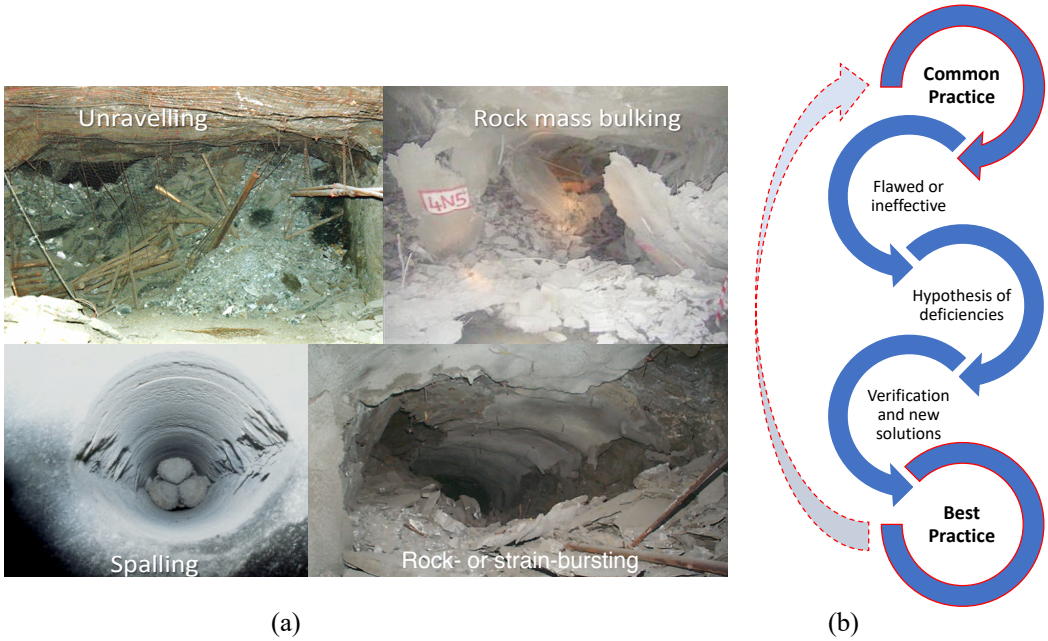


(a) (b)

Figure 1 (a) Examples of excavation instabilities in stressed rock suggesting flawed or ineffective solutions based on common practices, and (b) path of discovery to arrive at better and best practices.

Because many engineering approaches and common practices are flawed or ineffective, and may even be obsolete, best practices have to be developed based on hypotheses of the underlying causes for the deficiencies (Fig.1b). Once these hypotheses have been verified by testing and field observations, improved solutions can be found and implemented. Eventually, new knowledge and experiences may be acquired and the innovation cycle may restart as indicated in Figure 1b.

Rather than elaborating on flaws of common practices, this lecture focuses on best practices in three key areas of rock engineering for safe and cost-effective underground mining and construction:

- Excavation vulnerability and fragility assessment;
- Rock mass behavior and characterization for rock mass strength determination; and
- Ground control and support selection.

## 2 UNDERSTANDING EXCAVATION BEHAVIOR

Understanding excavation and rock mass behavior is a prerequisite for successful rock engineering and therefore for the development of best practice guidelines.

### 2.1 *Excavation failure mechanisms*

Only if all potential excavation failure mechanisms (Fig.2a) are understood can the vulnerability of an excavation to failure and the potential severity (extent or violence) of damage be anticipated, and the resulting critical load, displacement and energy demands be established (by empirical, analytical, or numerical modeling). Because of the author's recent experience from major mining (caving) operations, this lecture is built on lessons learned from moderate to severe excavation instabilities in mining. The cartoon-like images illustrate the four mechanisms described in the figure caption.

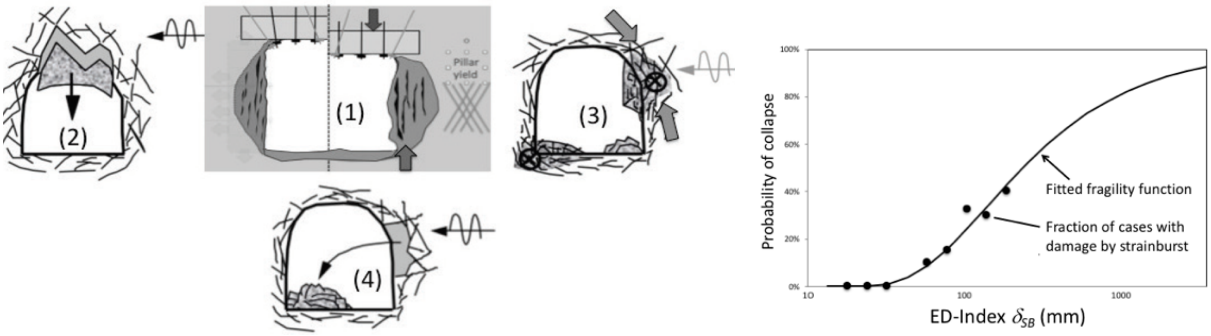


(a) (b)

Figure 2 (a) Failure mechanisms for (1) static loading causing stress fracturing (spalling), (2) gravity-driven failure (incl. shakedown), (3) bulking-driven failure (incl. strainbursts), and (4) energy-driven failure (incl. stress wave reflection, etc.); and (b) Generic example of a fragility curve defined by the ED-index $\delta_{SB}$ for damage by strainbursts (3).

#### 2.1.1 *Defining safety margin – Vulnerability assessment*

By comparing load, displacement and energy demands to the capacity of rock support systems, the proximity to failure, i.e. the probability of failure or factor of safety, can be assessed and appropriate support systems can be selected. In this manner, the vulnerability of an excavation to failure is described by answering the question 'How close is it to failure?', i.e. 'How full is the glass?' for each of the four failure modes shown in Figure 2a.

In rock engineering, depending on the anticipated excavation behavior, one or more of the following three Factor of Safety (FS) have to be assessed:

$$FS_{Load} = \frac{\text{Support Load Capacity}}{\text{Load Demand}} \qquad \text{(e.g. for (2) in Fig.2a)} \qquad (1)$$

$$FS_{Disp} = \frac{\text{Support Displacement Capacity}}{\text{Displacement Demand}} \qquad \text{(e.g. for (3) in Fig.2a)} \qquad (2)$$

$$FS_{Energy} = \frac{\text{Support Energy Capacity}}{\text{Energy Demand}} \qquad \text{(e.g. for (4) in Fig.2a)} \qquad (3)$$

Once the vulnerability is established, more questions arise: 'How severe or violent will the failure be?', i.e. 'How much water will spill?', or 'How fragile is the excavation?' The fragility of an excavation describes the likelihood of damage at a defined severity, e.g. in terms of volume or weight of displaced rock, cumulative displacement imposed on the support, or the violence of energy release.

In other words, critical Engineering Demand (or Design) Parameters (EDP) have to be selected to establish the vulnerability and fragility of an excavation. The development of best practices therefore starts with the identification of dominant EDPs (Kaiser & Cai, 2019).

The vulnerability of an excavation describes the state of exposure to physical damage. Strictly speaking, it is the probability of damage to occur at a given site without consideration of the severity of the resulting damage. The vulnerability assessment aims at identifying potential damage locations, evaluating design issues against various types and levels of threat (mining-induced stress, ground motions in burst-prone mines, etc.), and determining levels of protection by mitigation measures.

### 2.1.2 *Defining damage potential - Fragility assessment*

The *fragility* (antonym: robustness) is a measure of how easily an excavation can be broken or how much damage is caused. It is the probability of an undesired outcome (a specified damage level, e.g. R1 to 5 (Potvin et al. (2009)) as a function of excitation, i.e. a particular excavation demand parameter (EDP) or a combination of EDPs (e.g. advancing stress front, extraction ratio, ground motion, etc.).

An excavation may or may not be vulnerable to damage for a given load, displacement or energy demand, but it may be more or less fragile (or robust). Vulnerable excavations are likely to be damaged but robust excavations will suffer less damage than fragile excavations.

Once a deficiency in a common practice has been identified, the first step is to establish a hypothesis of how to overcome it (Fig. 1b) and how to identify critical EDPs that are needed to characterize and assess the vulnerability and the fragility.

### 2.1.3 *Identification of critical EDPs*

In earthquake engineering, fragility curves are used as a statistical tool to identify the probability of exceeding a given damage state or a threshold as a function of specific engineering demands. For earthquakes, this demand is often represented by the ground motion (preferably spectral displacement at a given frequency). A fragility curve is a graph with the demand (horizontal axis) defined by a representative EDP (e.g., peak ground velocity or acceleration (*PGV* or *PGA*), mining-induced stress, dynamic stress wave increments, etc.), and the probability of a defined damage level (cracked shotcrete, failed bolts, etc.) on the vertical axis. When the damage severity is affected or dominated by multiple factors, the fragility has to be defined based on an Engineering demand index (ED-index) that considers the relative contribution from all relevant demands.

The same concept can be applied to static demands (loads or displacements). Some examples of EDPs or ED-indices are listed below:

- EDPs for $FS_{Load}$: Geological structure geometry for wedge volume or weight estimation, or an ED-index linking the stress level *SL* for depth of failure $d_f$ estimations to the weight of stress-fractured rock;
- EDPs for $FS_{Disp}$: an ED-index reflecting the peak and post-peak strength of the rock mass and its dilation or rock mass bulking behavior;

and for rockbursting ground:

- EDPs for $FS_{Energy}$: ground motions (*PGV* or *PGA*) for damage dominated by strong remote seismic events (e.g. shakedown from seismic events or earthquakes) and, for strainbursts, an ED-index combining stress level *SL*, the depth of strainbursting $d_{SB}$, the bulking factor, and stored strain energy.

For example, when assessing the fragility to spalling (subscript S) or self-initiated strainbursting (subscript SB), the severity of damage by excessive bulking of stress-fractured rock can be described by an ED-index that reflects the displacement demand:

$$\delta_S \; or \; \delta_{SB} = d_f \bullet BF = (b\,SL - c) \bullet a \bullet BF \qquad (4)$$

where, $d_f$ = depth of failure, static $SL = (3\sigma_1 - \sigma_3)/UCS = \sigma_{max}/UCS$, $a$ = the equivalent tunnel radius, and $b$ and $c$ are constants ($b$ = 1.37 and $c$ = 0.42 for static loading; for dynamic loading see Kaiser

(2006))[2]. For dynamically loaded strainbursts, the stress level is temporarily increased to $SL_{SB} = SL+\Delta SL_d$, where $\Delta SL_d$ reflects the change in SL due to dynamic loading of the excavation (Kaiser et al. 1996).

A generic example of a fragility curve for the strainburst severity is presented in Figure 2b (note: log-scale for EDP = strainburst displacement). In this case, there is a 40% probability of collapse by a strainburst if the displacement induced by the strainburst reaches 200 mm. The vulnerability to strainbursting is largely controlled by the rock mass's stress to strength ratio (or *SL*) and the fragility is dominated by the depth of failure (static plus dynamic) and the bulking factor (Eqn 4).

For relatively small seismic events, the fragility is not or only vaguely related to the ground motion (Kaiser & Cai, 2019). Hence, fragility curves for strainbursts have to be developed in terms of load, displacement, and energy release demands (excluding *PGV* or *PGA* as they only trigger the failure process and do not contribute to the severity of damage).

For falls of ground or seismically triggered shakedown failures, respectively, gravitational and dynamic accelerations (ground motions measured by representative *PGA*) define the demand and the fragility is controlled by the brittleness of the support system. An ED-index reflecting the ground motion and ductility of the support is therefore needed to assess the fragility of an excavation to shakedown failure.

*From common to best practice*

Identification of EDPs is a prerequisite to determine whether common practices are applicable or flawed. For excavation design and support selection, EDPs or ED-indices characterizing vulnerability and fragility must be clearly identified and then used to recognize potential failure modes to obtain relevant rock mass parameters.

### 2.2 *Static failure modes of unsupported excavations*

Under static loading, the excavation behavior can be characterized by two dominant EDPs as illustrated by the 3 × 3 excavation behavior matrix presented in Figure 3 (modified from Kaiser et al. (2000) and presented by Kaiser (2017) and Kaiser & Cai (2019). The horizontal axis represents the EDP = Rock Mass Quality (RMQ) or rock mass strength and the vertical axis the EDP = stress level.

The rock mass quality (RMQ) is grouped: RMQ1 for massive to discontinuously jointed rock, RMQ2 for fractured and blocky to disintegrated ground, and RMQ3 for weak and soft, highly fractured or sheared rock. The boundaries have been slightly adjusted from Kaiser et al. (2000) based on experiences with excavation failures at depth to:

- 40 > Q' < 40; with Q' = modified rock tunneling quality index Q for $J_w/SRF = 1$;
- 75 > RMR (Rock Mass Rating) < 75; or
- 70 > GSI (Geological Strength Index) > 70).

The stress intensity is defined on the left side if Figure 4a by the in-situ stress to strength ratio $\sigma_1/\sigma_c$ and on the right by the stress level $SL = \sigma_{max}/UCS$. Using the stress level as an EDP is beneficial as the impact of the in-situ stress ratio $k = \sigma_1/\sigma_3$ or mining-induced ratio $k_m = \sigma_{1m}/\sigma_{3m}$ is accounted for. This distinction is particularly relevant when mining changes the mining-induced stress field, and failure modes may change, e.g. from $M_2$ to $M_1$ due to relaxation.

[2] $\sigma_{max} = 3\sigma_1 - \sigma_3$, with $\sigma_1$ and $\sigma_3$ representing the in-situ, or mining-induced major and minor principal stresses ($\sigma_{1m}$ and $\sigma_{3m}$), in the vicinity of the tunnel in a plane perpendicular to the tunnel axis. $\sigma_{max}$ represents the excavation-induced stress at the location with the highest tangential stress near the wall of an equivalent circular excavation in elastic rock. The stress level *SL* as a EDP is therefore an index rather than a measure of the actual stress to strength ratio. When mining changes the stress field near a tunnel the stress level *SL* changes. The combined effect is called 'mining-induced stress' and is used on the right scale of Figure 3a. This approach does not account for the intermediate principal stress that may affect the failure mode, e.g., at or near the tunnel face or near intersections.

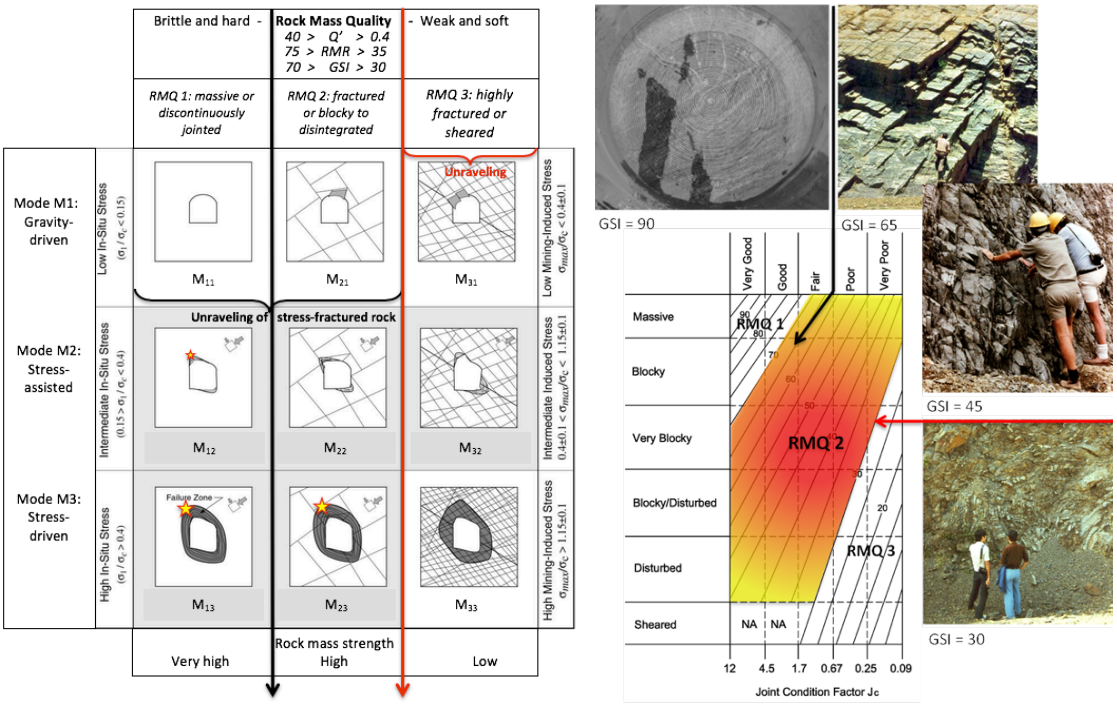


(a) (b)

Figure 3 (a) Excavation behavior matrix showing expected rock mass failure modes $M_{11}$ to $M_{33}$ as a function of rock mass quality (RMQ) or strength, and in-situ stress (left scale) or the excavation- and mining-induced stress (*SL* scale on the right) (modified from Kaiser et al. (2000)). The red and black arrows link to (b) the corresponding rock mass quality in the Geological Strength Index (GSI) chart (Kaiser (2017) and Kaiser & Cai (2019) with images courtesy E. Hoek).

*Excavations in massive to discontinuously jointed rock masses are prone to stress fracturing near the excavation:*($M_{11}$: Elastic response; $M_{12}$: Localized brittle failure of intact rock adjacent to excavation boundary; $M_{13}$: deep brittle failure of intact rock; potentially surrounding the entire excavation.)

Failure modes with localized spalling or stress-fracturing are observed once the stress level $SL = \sigma_{max} / UCS$ exceeds 0.3 to 0.5 ($M_{12}$ and $M_{13}$) or 0.25 to 0.35 in defected or veined rock (Bewick et al. 2019). At intermediate mining-induced stress levels ($SL \leq 1$), the fracture zones typically remain localized (i.e. notches form). The stress-fractured zone becomes continuous in rock masses with low tensile strength at very high stress levels and when *k* is approaching unity.

Strainbursting may occur at the excavation wall or at some distance from the wall as indicated by the stars in Figure 3a. They occur at the interface between the excavation damage zone and the more competent elastic rock mass surrounding it. Furthermore, they may occur in supported rock and in rock of quality RMQ2 if joints are oriented such that shear slip is prevented along these joints. Consequently, as the depth of stress-fractured ground increases, excavations become increasingly more vulnerable to falls of stress-fractured ground and to strainbursting. According to Barton & Grimstad (1994), minor bursting (rock 'spitting') is to be expected during a tunnel advance at excavation-induced stress levels $SL > 0.65$ and severe rockbursting is to be anticipated, largely due to larger burst volumes, at $SL > 1.0$.

*Excavations in fractured or blocky to disintegrated rock masses are prone to failure with some structural controls:* ($M_{21}$: Falling or sliding of rock blocks and wedges; $M_{22}$: Localized brittle failure of (weak) intact rock blocks bound by open discontinuities or joints that facilitate movement of rock blocks; $M_{23}$: Brittle failure of intact rock around an entire excavation combined with movement of rock blocks bound by open joints.)

At low stress, this rock mass requires support. At elevated stress ($M_{22}$ and $M_{23}$), blocks formed by open joint sets tend to fracture near excavations due to extension straining caused by stress heterogeneities. As a consequence, the natural block size is reduced and the rock mass becomes prone to unraveling. The extent of rock mass disintegration increases with depth and the resulting rock mass damage zone is prone to failure involving interactions with natural joints. The EDPs are typically defined by the depth of failure. In hard brittle rock, geometric bulking (due to a geometric non-fit of rock blocks

or fragments) may impose large deformations on the support. The safety margin is best assessed in terms of an EDP describing the displacement demand.

*Excavations in highly fractured or sheared ground are prone to falls of ground, unraveling and excessive plastic deformation*: ($M_{31}$: Unraveling of blocks from the excavation surface; $M_{32}$: Localized failure of rock, weak blocks bound by open joints, and unraveling along discontinuities; $M_{33}$: Squeezing in an elastic/plastic continuum with or without swelling potential.)

At elevated stress levels (modes $M_{32}$ and $M_{33}$), the behavior is further characterized by stress-driven plastic yield (Martin et al. 2003). This rock mass class (RMQ3) always requires support with a robust retention system (e.g. mesh and shotcrete) to prevent unraveling between bolts. The dominant EDPs are load-demands in $M_{31}$ and deformation demands in $M_{32}$ and $M_{33}$.

Four typical images of rock mass qualities covering the range of rock mass quality from RMQ1 to RMQ3 are shown in Figure 3b together with applicable ranges in the GSI chart.

As indicated earlier, best practices must be simple but reflect all essential and dominant EDPs. For the identification of potential excavation failure modes and for the determination of relevant EDPs, unnecessary complexities can be eliminated and the rock mass can be, as suggested by Terzaghi (1946), characterized by block size (with boundaries at 10 cm and 1 m on the GSI scale; Fig. 4) and joint condition (with boundaries at $J_c$ = 3 and 0.25; Fig. 3b).

For the selection of appropriate rock engineering approaches, it is, in order of priority, necessary to:

- identify whether the intact rock strength dominates: RMQ1 versus RMQ2 or 3.
  According to Figure 4, in 'good' rock masses the key EDPs relate to the intact rock and rock block strength. The block size does not matter and engineering methods applicable to blocky rock mass models are not suitable (see discussion on applicability of GSI-strength equations in Section 5.1.1).
- identify whether inter-block characteristics dominate: distinguish RMQ2 from RMQ3.
  According to Figure 4, definitions of what constitutes poor ground vary widely.
  - In RMQ2, interlock contributes to the rock mass strength and the key EDP describes the block size as it dominates the excavation behavior (e.g. unraveling depends on excavation size).
  - In RMQ3, the characteristics of infilling dominate and the joint condition becomes the key EDP. Recognizing this sensitivity led to the development of the GSI with particular focus on weak and soft rock (Hoek et al. 1995).

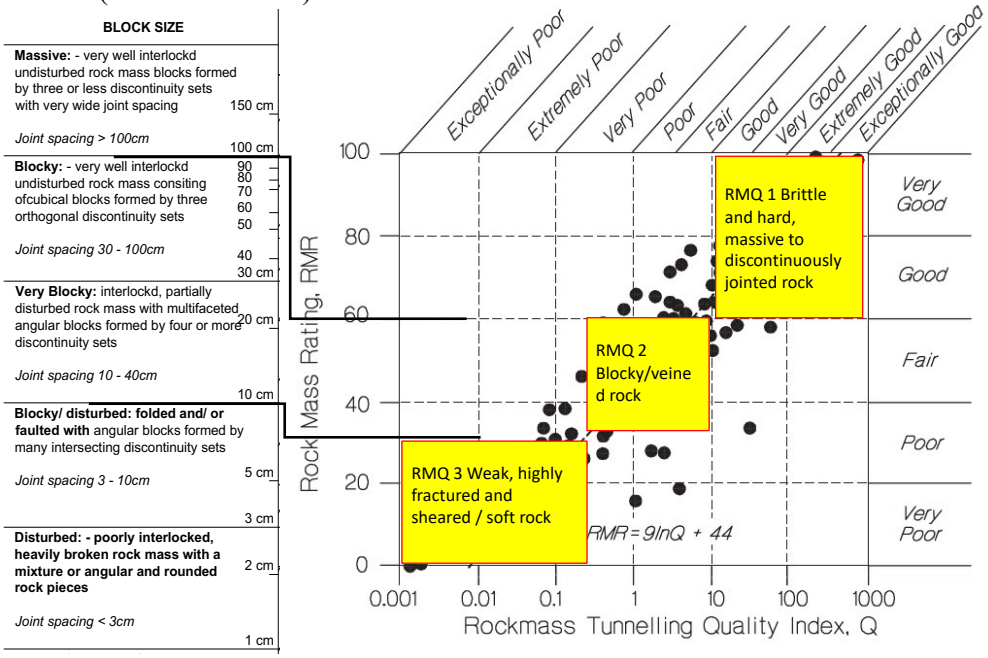


Figure 4 Rock mass quality grouping for excavation failure and EDP selection. Left: GSI block size description. Right: simplified grouping of rock mass quality RMQ1 to 3 superimposed pm chart from Hutchinson & Diederichs (1996) with linear trend after Bieniawski (1979).

*From common to best practice – failure under static loading*

Excessive effort is often expended in common practice to collect and rate rock mass details that have little impact on the excavation behavior and consequently on a design. Meanwhile, dominant factors, e.g. persistence, veining, and rock alteration, are either ignored or underrepresented.

Best practices must ensure that rock mass quality classes RMQ1 to 3 and the stress level *SL* as well as its evolution over the duration of a project are properly defined. In mining, it is particularly important to reflect on the stress path causing changes in the *SL* that may lead to changes in failure modes. For example, relaxation may move the failure mode from $M_{22\text{ or }23}$ to $M_{21\text{ or }31}$; whereas an increase in extraction ratio may move it from $M_{22\text{ or }32}$ to $M_{23\text{ or }33}$. Both may drastically change the support requirements and render common practices in support selection as inapplicable.

### 2.3 *Dynamic failure modes of unsupported excavations*

By comparing Figure 2a to Figure 3a, it follows that dynamic disturbances from earthquakes or mining-induced seismic events can lead to (a) strainbursts (in $M_{12\text{ to }13}$ and $M_{23}$) and (b) to seismically induced falls of ground or shakedowns (in $M_{31\text{ to }33}$ and $M_{22\text{ to }23}$). This is illustrated by Figure 5. The listed EDPs depend on the respective failure mode (see Section 2.3.3).

#### 2.3.1 *Shakedown damage*

For shakedown, there are two phases to consider: (1) the fall is initiated or triggered, and (2) the support dissipates the kinetic energy of the falling mass until a new equilibrium is established. If unsupported, the trigger limit defines the failure point. If the support is effective, it survives the load and kinetic energy of the falling rock (thus called survival limit). For more details on shakedown failure analysis, the reader is referred to Chapter 8 in Kaiser et al. (1996).

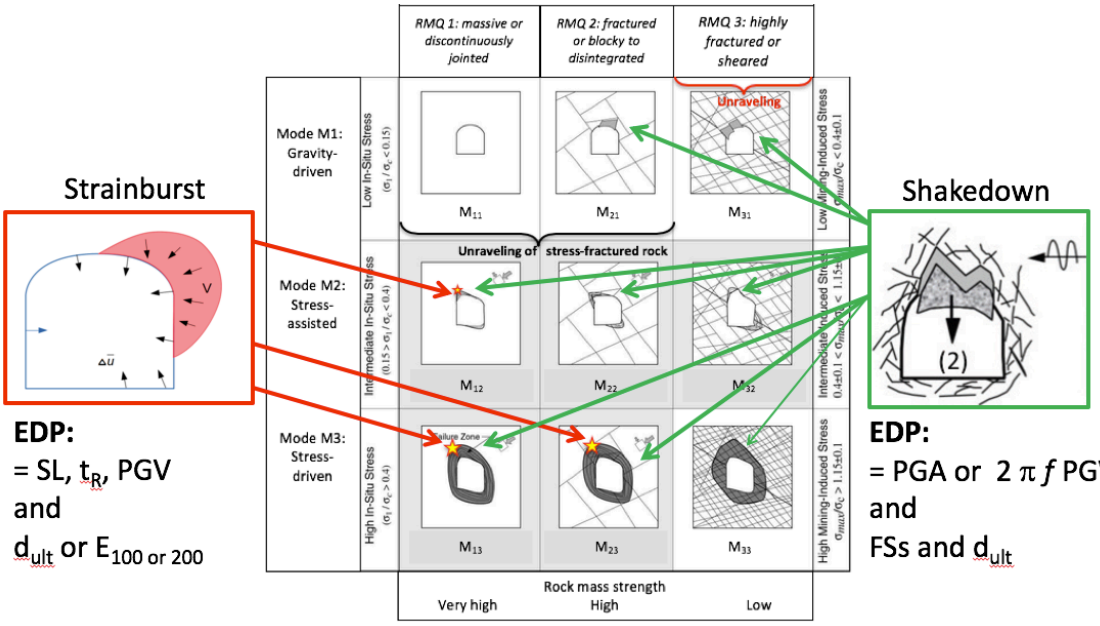


(a) (b)

Figure 5 Excavation behavior matrix with two predominant dynamic failure modes: (a) strainburst, and (b) shakedown.

#### 2.3.2 *Strainburst damage*

Strainbursts are sudden, violent failures of the rock mass in a 'burst volume' near an excavation. They occur in highly stressed rock, often at stress raisers as illustrated by Figure 6a (in red), i.e., at the transition from damaged to relaxed ground (in blue) or at locations of elevated stress due to geological structures. The burst process, simulated by Gao et al. (2019a, b), involves the creation of new fractures and rock fragments. These cause a sudden geometric bulking in the burst volume and an associated inward movement of the wall $\delta$ that is equal to the depth of strainbursting $d_{SB}$ times a representative bulking

factor *BF*. This inward movement directly loads the support components at the plate and causes indirect loading or straining of tendons that penetrate the burst volume and the undamaged rock beyond.

The violent wall displacement may cause rock ejection if the burst volume and the 'burden' of relaxed rock (shown in blue in Fig. 6b) is not effectively supported. The bulking velocity $v_B$ at the inner edge of the burst volume depends on the time of rupture $t_R$ (the time it takes to fail the burst volume). The initial velocity can be approximated by $v_B = \delta / t_R$. It eventually reduces to zero if the rock is effectively supported. If not, some rock and support components may be ejected at velocities $v_{ej}$ less than $v_B$.

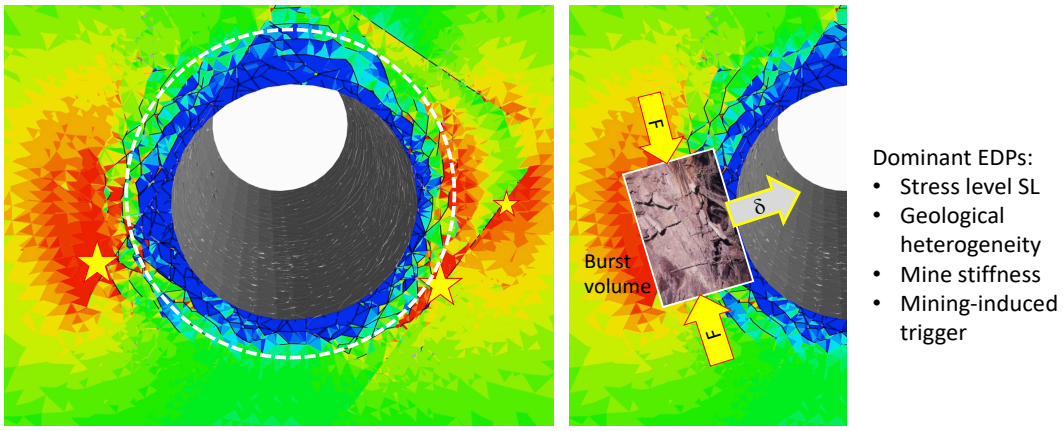


(a) (b)

Figure 6 (a) The major principal stress contours (relaxed zone in blue and stress raisers in red). Potential strainburst locations are indicated by stars (Discrete element model by Garza-Cruz et al. (2015) and Pierce (2016; pers. com.); (b) stress-fractured rock in burst volume driven by tangential forces $F$ causing radial wall displacement $\delta$. Dominant EDPs are listed.

*Types of strainbursts*

There are three types of strainbursts:

- *Self-initiated strainburst* where excavation damage is caused by the release of stored strain energy when the mining-induced stress (load) exceeds the supported rock mass capacity;
- *Seismically triggered strainburst* where a stress wave from a remote seismic source initiates the failure (triggers the same damage process as above; the remote event adds little or no energy); and
- *Dynamically loaded strainburst* where the stress wave from a remote seismic source causes a substantial dynamic stress change[3] deepens the zone of stress-fractured rock to $d^d_{SB} = d_{SB} + \Delta d_{SB}$, and adds kinetic energy, thereby increasing the damage severity.

Stored strain energy, in and around the burst volume (intrinsic and relative brittleness; Tarasov & Potvin(2012)), is a prerequisite for strainbursting. For vulnerable excavations, the burst volume is brought to failure by the tangential stresses near an excavation reaching the local rock mass strength. The severity of the damage from a self-initiated strainburst is related to the strain energy stored in the bust volume (depending on the intrinsic stiffness) and the energy released from the surrounding rock mass (depending on the relative stiffness or the loading system stiffness). In other words, the severity of strainbursting is dominated by the brittleness of the rock mass and the loading system stiffness. The severity is only related to the energy release from large remote seismic events if the magnitude $M_L > 2$ (dynamically loaded strainbursts; Kaiser & Cai, 2019).

### 2.3.3 *EDP for dynamic failure processes*

The most relevant EDPs for the assessment of the vulnerability and the fragility of excavations to dynamic failures are listed in Table 1.

[3] Ortlepp (2005) suggested that strainbursts with $M_L$ = -0.2 to 0 are usually undetected but that buckling bursts (also caused by stored strain energy release) generate seismic events of $M_L$ = 0 to 1.5. For mining, Kaiser & Cai (2019), based on data by Morissette et al. (2012), show that seismic events of magnitudes $M_L < 1.5$ to 2 at a distance $R > 10$ m add insufficient energy to affect the severity of strainbursts.

Table 1 EDPs for dynamic failure modes (2) to (4) in Figure 2a.

| | Static *FSs* | Stress level *SL* | Support ductility $d_{ult}$ | Ground motion PGV | Strainburst rupture time $t_R$ (ms) | Bulking factor $BF(p_s)$ | Note |
|---|---|---|---|---|---|---|---|
| Shakedown<br>Unsupported<br>Supported | <br>√ | √ | <br>√ | √ | | | Always check load capacity |
| Loose rock or shotcrete **ejection** | FSs = 1 | | | $(n*PGV)^2$ | | | Use mesh to hold fragments |
| **Spalling** by tangential stress increment | FSs = 1 | √ | | n*PGV | | | Use mesh or shotcrete to retain fragments |
| Triggered strainburst (energy and displacement) | √ | *FSs* = 1 dominates $d_{SB}$ (burst volume) | √ | | √ dominates severity or violence | √ dominates displacement severity | Select support system to survive displacement and energy |
| Dynamically loaded strainburst | √ | √ | √ | √ Adds $\Delta SL = f(PGV)$ | √ | √ | Select support system to survive displacement and energy |
| Momentum transfer | √ | √ | √ | √ | | √ | Design for large events $M_L > 2$ |

Depending on the dominant failure process, different EDPs need to be considered. With reference to Figure 2a:

- For failure mode (2), i.e. shakedown, the weight (gravitational force) is enhanced by dynamic forces caused by dynamic acceleration. Ground motions from a remote seismic event (*PGA* or *PGV*) are controlling EDPs for failure initiation, i.e. for vulnerability assessment of unsupported excavations. If supported, the survival limit (Kaiser et al. 1996) depends on the static factor of safety $FS_s$ before the shakedown event, and the ductility of the support, i.e. the remnant displacement capacity of the support at the time of dynamic loading.
- For failure mode (3), i.e. dynamic bulking failure during a strainburst, the wall displacement $\delta^d_{SB}$, which may depend on the ground motions *PGV* (if $M_L > 2$) and the bulking velocity $v_B = \delta / t_R$, are the controlling EDPs.
- For failure mode (4), i.e. dynamic stress reflection or energy-enhanced or -driven failures by strong or close seismic (fault slip) events, causing ejection or shakedown of loose rock or poorly bonded shotcrete (shotcrete rain), the ground motions *PGV* is the controlling EDP (not covered here).

*From common to best practice – dynamic failure*

Common ground-motion-centric or pure energy-based support selection with *PGV* as a single EDP ignores or underestimates the often dominant rock mass bulking process near the excavation as well as the associated displacements. These displacements cause direct and indirect impact loading of support components. Best practices have to consider the impact of pre-burst support deformation and bulking displacements during the burst (see Section 6).

When dynamic failure processes are triggered, energy can be released from the burst volume, i.e. "when the glass is full, the severity of damage depends on the size of the reservoir". Other EDPs, such as rupture time and bulking factor as well as the static factor of safety and support ductility, have to be considered (Kaiser et al. 1996).

## 3 REPRESENTATIVE ROCK AND ROCK MASS BEHAVIOR FOR DESIGN

Once the excavation behavior and failure processes are understood and relevant EDPs are identified, the designer has to obtain representative rock mass strength envelopes and then capture the rock and rock mass behaviors using representative yield or failure criteria.

### 3.1 *Rock strength or failure envelopes*

If the rock or a rock mass behaves like a cohesive and frictional material (soil), the linear Mohr–Coulomb failure criterion, specifying that the shear strength is composed of two simultaneously mobilized strength components, cohesion and frictional strength, is applicable:

$$\tau = c + \sigma' \tan \phi \tag{6}$$

As Schofield (1998) pointed out, strain affects the two strength components differently even in soil tests, rendering Eqn 6 inapplicable for materials with interlock and with strain-dependent cohesion. Consequently, Eqn 6 is not valid for intact rock or interlocked rock masses. It is only applicable for failure mode $M_{33}$ in RMQ3.

*The Mohr–Coulomb error*

Schofield (1998), by reference to Taylor's work and to Terzaghi's use of the Mohr–Coulomb (MC) criterion, pointed out that it is a serious error to assume that the cohesion and frictional strength are simultaneously mobilized. He correctly concluded "In adopting the Mohr–Coulomb equation Terzaghi made the error of regarding apparent cohesion as a soil property independent of strain". Based on work by Martin (1997), it is now well-understood that the mobilization of the cohesive and frictional strength components of rock and rock masses is strain-dependent. Accordingly, Coulomb's strength equation needs to be rewritten as shown below with cohesion, 'effective' stress internal to the rock, and the dilation angle depending on the plastic strain $\varepsilon_p$:

$$\tau = c(\varepsilon_p) + \sigma'(\varepsilon_p) \tan(\phi + i(\varepsilon_p)) \tag{7}$$

As a consequence, rock mass failure forecasting becomes highly sensitive to the assumed stress–strain characteristics. For rock engineering applications, Schofield's statement can be paraphrased as 'adopting the Mohr–Coulomb equation and regarding apparent cohesion as a rock property independent of strain is a serious error'. Overcoming this deficiency is an essential step to move from common to best practice. Unfortunately, common practices of using elastic-perfectly brittle models ignore this and often lead to predictions of excessive depth of yield. Best practice strength models have to properly represent the gradual transition from peak toward the residual strength. The word 'toward' is intentionally used here to highlight that the residual strength is rarely reached in underground construction (see Section 3.1.6 on post-peak strength).

#### 3.1.1 *Peak strength envelopes*

Recognizing the nonlinearity of triaxial test data (in the $\sigma_1 - \sigma_3$ space) and the need for a tension cut-off led to the development of the now commonly adopted Hoek–Brown strength envelope for rock and rock masses. The resulting peak strength equations are also independent of strain (as in Eqn 6) for MC criterion) and thus provide best-fit envelopes to peak strength data.

Based on a careful examination of the low confinement range of most brittle rocks, Kaiser & Kim (2014) introduced an s-shaped peak strength envelope to better represent the cohesion loss at low confinement due to extensional cracking, and the high strength gain near the spalling limit due to high dilation. The resulting equations for the s-shaped peak strength are again independent of strain but provide more representative peak strength envelopes for brittle rock (see Section 3.1.2 concerning elevated HB parameters).

*Unconfined compressive strength (UCS)*

While the UCS test is one of the most common index tests for site characterization, producing meaningful results remains a challenge. The indiscriminate use of UCS data without careful screening of failure modes may mislead when used in rock mass classifications, semi-empirical depth of failure estimations, TBM penetration rate charts, or when determining rock strength envelopes.

Bewick et al. (2015) reviewed critical factors impacting the UCS[4] and provide guidance for processing and the interpretation of UCS test data from homogeneous to heterogeneous rock. Common practice of UCS testing typically leads to (excessively) high variability in test data: coefficients of variation (CoV) generally exceed 25% for homogeneous rock and 35% for heterogeneous rock. This variability can be attributed to variations in specimen failure modes in heterogeneous rock. To improve consistency, testing must be carried out by a qualified laboratory using appropriate QA/QC procedures, and the ISRM suggested or ASTM methods. Best practices as outlined by Bewick et al. (2015) need to be adopted:

- The UCS for homogeneous rock should be based on 5 to 10 or more intact specimens; filtering of test data is required to get the intact strength of the homogeneous component of rock blocks.
- For heterogeneous rock a minimum of 10 to 40 specimens are required.
  - If the CoV exceeds 30 to 35%, the data are likely bi- or even multi-modal due to unique characteristics. Respective mean strength values should be defined for sub-datasets (e.g. Fig. 7).
  - The complete dataset is representative of the strength and variability of a heterogeneous rock block.
- Depending on the empirical design approach, either the homogenous or the heterogeneous UCS or both may be relevant; e.g. for the stress level to establish the depth of spalling, the mean UCS for the homogeneous specimens should be used (Martin 2019).

An example is presented in Figure 7. The mean UCS = 120 MPa with an excessive CoV = 59% suggests that the sample population consisted of at least two populations. After identifying specimens that mostly failed with intact rock breaks, the bi-modal distribution shown in green was derived with a mean UCS = 220 MPa for the homogeneous part and 96 MPa for the heterogeneous part. The practical implications of ignoring the bi-modal nature can be serious. For example, the disk consumption may be unexpectedly high and the TBM penetration rate may be severely compromised if estimates are based on mean UCS-values for the entire sample population. The extreme values defining the homogeneous rock strength will dominate the disk performance.

Best practices in UCS data testing and reporting must include filtering of UCS data by failure mode separate homogeneous and heterogeneous data.

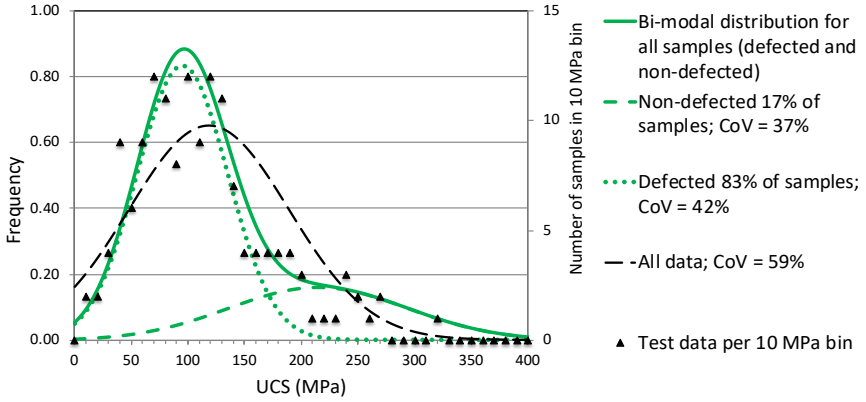


Figure 7 Frequency distributions for a heterogeneous, brittle Quartzite.

### 3.1.2 *S-shaped failure envelope for brittle rock*

As indicated above, Kaiser & Kim (2008, 2014) introduced the s-shaped or tri-linear peak strength envelope concept to better represent the rock strength in the low confinement range (Fig. 8a). For the example shown in Figure 8b, the mean UCS (or $UCS_I$) depicts the average expected UCS in the low confinement range ($\sigma_3 < UCS/10$). The apparent AUCS (or $UCS_{II}$) provides the y-intercept of the shear strength envelope at higher confinements. The transition occurs at the spalling limit $k_s = \sigma_1/\sigma_3$ ($k_s = 15$ in this case).

When numerical modeling tools do not facilitate s-shaped or tri-linear failure envelopes, it is necessary to approximate the s-shaped peak strength envelope by selecting appropriate Hoek–Brown (or

[4] Note: $UCS \neq \sigma_{ci}$, the Hoek-Brown unconfined strength parameter (Kaiser & Kim (2014).

Mohr–Coulomb) parameters. As illustrated by Figure 8c (Kaiser & Kim, 2014), uncommon high $m_i$-values emerge ($m_i$ = 72 in this case). Similarly, if MC parameters were fitted, abnormal high slopes ($\phi + i$) would appear in the low confinement range.

Best practice for such materials is to ignore common Hoek–Brown parameter tables (with $\sigma_{ci}$ and $m_i$ = 24 for Quartzite; Hoek et al. (1995)) and to adopt a representative mean UCS-value (e.g. 95 MPa) and a high, best fit $m_i$-value (e.g. $m_i$ = 72).

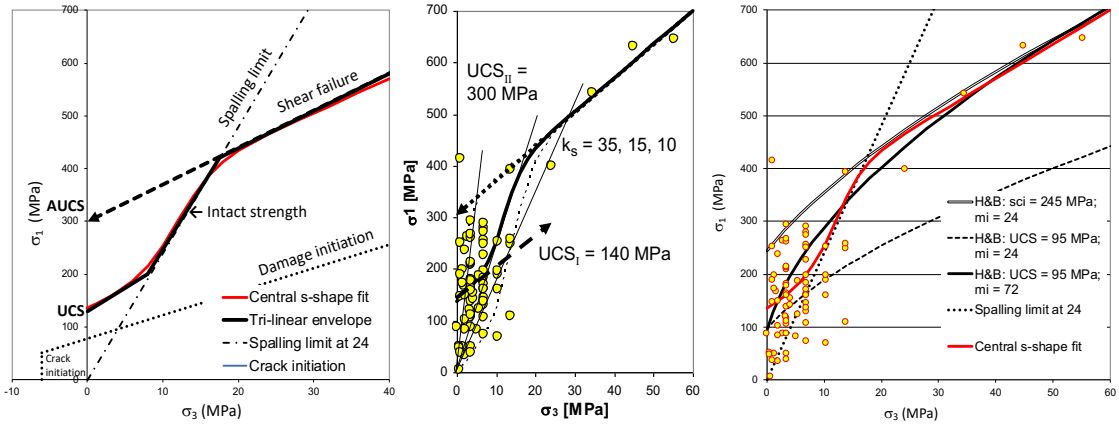


(a) (b) (c)

Figure 8 (a) Schematic tri-linear failure criteria; (b) fitted s-curve (dotted for lower limit) with respective linearized approximations; and (c) Hoek–Brown envelopes obtained by various fitting approaches. The resulting parameters are shown in the legend, i.e., UCS and $m_i$ (modified from Kaiser & Kim, 2008).

### 3.1.3 *Post-peak strength (PPS)*

In soil mechanics, the term 'residual strength' was introduced to represent the shear strength at very large strains, e.g. for slope stability analyses. As indicated above (Eqn 7), the rock strength is strain-dependent, and cohesive and frictional strength components are mobilized at different rates (Martin 1997). Near underground structures, however, the actual plastic strains are rarely sufficient to reach the residual strength. This is illustrated on a triaxial test data set with a 1% axial post-peak strain limit (Fig. 9a; the equivalent s-shaped peak strength with AUCS = 250 MPa is shown in Fig.9 c). The Hoek-Brown peak strength is defined by UCS = 130 MPa and $m_i$ = 18.

At 1% strain and $\sigma_3$ < UCS/10 (Fig. 9a), the cohesion is lost and the PPS is defined by a high 'friction plus dilation' angle due to interlock ($k$ = 15 or $\phi + i$ = 55º). At higher confinements, the apparent cohesion AUCS(1%) = 65 MPa or $k$ = 3.3 for $\phi$ = 33º.

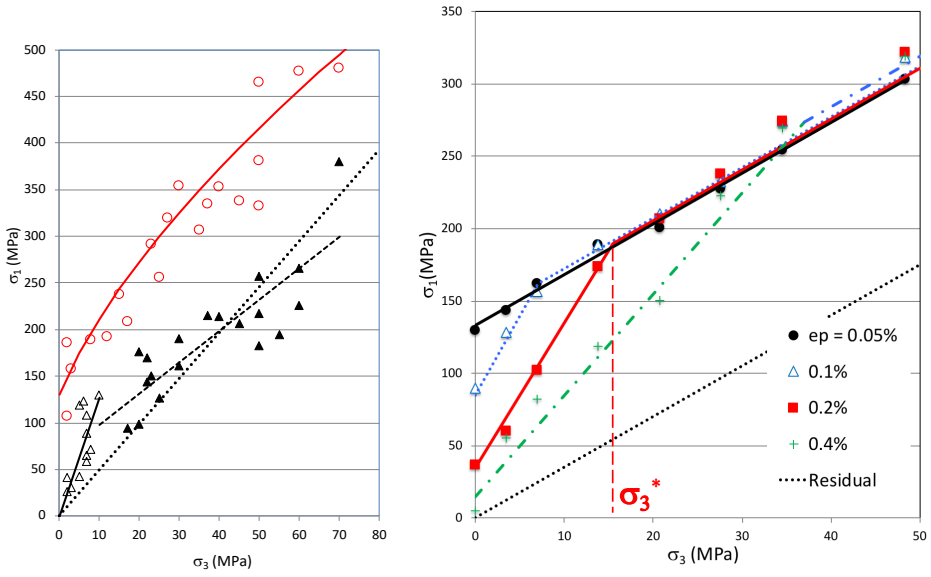


(a) (b)

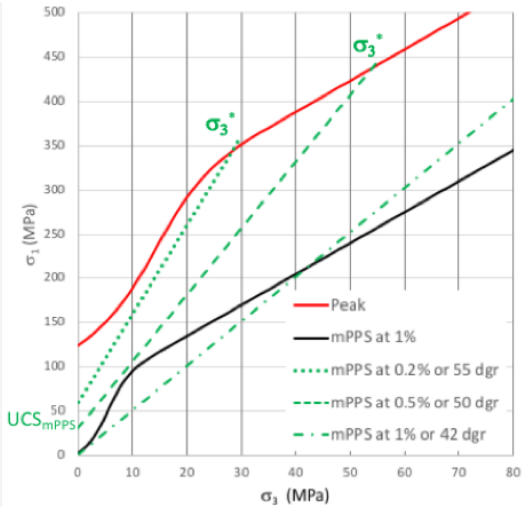


(c)

Figure 9 (a) Triaxial test data from tests on Quartzite (o for peak) with 1% axial strain limit (triangles); (b) bi-linear post-peak strength (PPS) envelopes for a Marble with brittle-ductile transition at $\sigma_3$* = 15 MPa for a plastic strain $\varepsilon_p$ = 0.2% (data from Wawersik & Fairhurst (1970)); the peak strength and three mobilized PPS envelopes are shown; residual at $\phi$ = 34º); and (c) s-shaped peak and mobilized post-peak strength (mPPS) at 1% strain for (a). Bi-linear mPPS envelopes with transitions at $\sigma_3$* = 22 and 60 MPa for 0.2 and 0.5%, respectively, are also shown.

For a Marble (Fig. 9 b modified from Kaiser (2016b)), the PPS is highly strain-dependent, leading to bi-linear mobilized PPS (mPPS) envelopes with a cohesion intercept and a change in the slope at a strain-dependent brittle ductile transition (at $\sigma_3$*). With increasing strain, the mPPS decreases and eventually reaches the residual strength. The cohesion intercept and the location of the transition point of the mPPS are strain-dependent and the residual strength is, for most rock types, only reached at very large strains, i.e. at strains that are rarely encountered in underground engineering, except close to an excavation boundary.

Whereas the transition from peak to residual can be steered in numerical models with appropriate constitutive laws, the residual strength should not be used as a bounding limit for underground rock engineering; except for RMQ3 and failure mode $M_{33}$, where the residual strength (Fig. 9b) may be reached. Rock failure simulations utilizing purely frictional post-peak strength envelopes, with the PPS set equal to the residual strength with zero cohesion, tend to underestimate the mobilized PPS and consequently lead to predictions of excessively large depth of yield. When elasto-perfectly brittle plastic transition models are used (e.g. with $RS^2$) strain-limited mPPS have to be adopted to prevent excessive loss of strength and yield zone propagation. It is recommended that the mPPS envelope honors three points as illustrated by Figure 9c: the tensile strength (not shown), $UCS_{mPPS}$ and the brittle-ductile transition point at $\sigma_3$*. For the Quartzite, the mPPS at 1% strain is represented by the s-shaped mPPS curve in Figure 9c. It can be approximated by a purely frictional mPPS with a slope of $(\phi + i)$ = 42º.

*From common to best practice*

Ample opportunities and economic as well as safety benefits can be derived by moving from common to best practices in rock strength determination. Common practices of fitting peak and residual strength data are clearly not best practice.

- Much care has to be taken to obtain representative UCS-values by identifying failure modes and separating homogeneous from heterogeneous specimen (Bewick et al. 2015).
- Failure envelopes are often s-shaped or tri-linear when cohesion and frictional strength components depend on plastic straining. This is valid for the peak and post-peak strength.
- Unless numerical models are calibrated to capture post-peak strength degradation, mPPS limits should be defined for anticipated plastic strain limits.

Figure 9c summarizes best practices in peak and mPPS definition for the test data shown in Figure 9a. For this case, the peak strength can be described by the conventional Hoek–Brown envelope (Fig. 9a ) or by a s-shaped envelope (Fig. 9c). The mPPS at small plastic strains exhibits a remnant cohesion (or $AUCS_{PPS}$ = 60 and 30 MPa) and a high slope $(\phi + i)$ ranging from 55 to 50º at 0.2 and 0.5% plastic

strain, respectively. At 1% plastic strain, the mPPS is bi-linear with $AUCS_{PPS}$ = 65 MPa and a slope angle of $\phi$ = 33° at $\sigma_3$ > 10 MPa.

### 3.2 *Rock mass behavior near excavations*

#### 3.2.1 *Failure criterion for brittle rock masses*[5]

As explained by Kaiser (2016a & b) based on work by Diederichs (2007), tensile stresses induced during deviatoric loading of heterogeneous rock lead to Griffith-type extension fracturing with the consequence of a depressed failure envelope (Fig. 10) in the low confinement zone where fracture propagation causing spalling is not suppressed by the available confining pressure. The resulting failure envelope for a rock mass is s-shaped and the stress space can be divided into two behavioral zones: spalling dominated stress fracturing at low confinement (to the left of the spalling limit), and shear rupture dominated behavior at high confinement (to the right). This divides the rock mass surrounding an excavation into two zones, an 'inner' and an 'outer' shell (Fig. 10).

#### 3.2.2 *'Inner' versus 'outer' shell behavior*

The threshold between the inner and outer shell is defined by the spalling limit, approximately near $\sigma_3$ = *UCS*/(10 to 15) as shown in Figure 10. From a practical perspective, there is a need to differentiate between engineering problems dominated by stress-fracturing (in the inner shell) and shear rupture (in the outer shell).

Inner shell engineering problems are those dominated by the behavior of the rock mass in the zone immediately surrounding an excavation where the confinement is low, i.e., in the zone where stress-fracturing can occur and blocks or fragment can rotate. Engineering challenges of support design, strainbursting, etc. fall into the class of inner shell problems.

On the other hand, engineering problems related to pillar instability, including pillar bursting, fall in the outer shell class where shear rupture dominates because spalling is partially or fully suppressed by sufficient confinement.

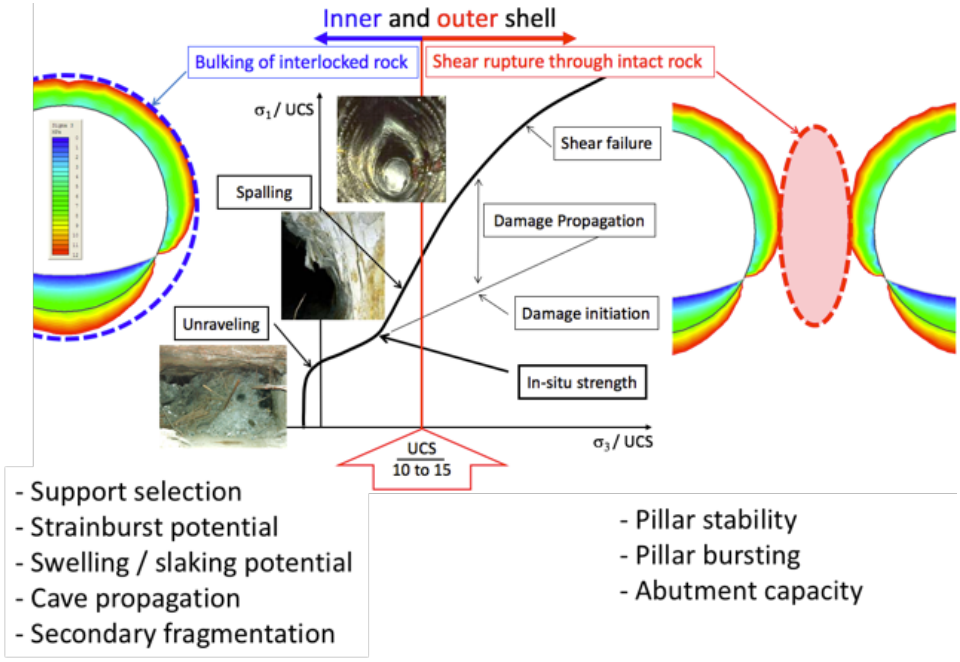


Figure 10 S-shaped failure criterion for brittle rock masses (center) and zoning of stress space for inner (left) and outer (right) shell behaviors in underground rock engineering (red contour $\sigma_3$ = 12 MPa).

[5] Strength envelopes define the rock strength (e.g. s-shaped envelopes) as obtained by testing, and failure criteria (e.g. bi-modal criteria by Diederichs (2007)) represent the rock or rock mass behavior for numerical modeling purposes.

### 3.2.3 *Depth of yield, failure and strainbursting*

*Depth of yield $d_y$*

Continuum models typically show indicators of yield and thus can be used to establish the depth of yield around an excavation (x in Fig.11; also shown are confining pressure contours for $\sigma_3$ = 0 to 10 MPa).

The three colored points (red, green, blue) in Figure 11 indicate that the rock at these locations still has a substantial cohesive strength and thus, while yielding, will not fall apart and will not fail under gravity loading alone, i.e. will not unravel. Only near the excavation, at locations with tensile failure (o), is the cohesion fully lost and unsupported rock would unravel. The depth of yield is therefore not the same as the depth of failure.

*Depth of failure $d_f$*

The depth of failure defines the depth to which a rock mass fails and unravels if unsupported. The normalized 'extreme' depth of failure $d_f^e/a$, i.e. the maximum depth of notch formation by spalling recorded in a tunnel domain with otherwise equal properties, increases linearly as a function of the stress level (up to $SL$ = 1 or $\sigma_\theta = \sigma_{max}$ = mean UCS (Martin 2019)).

The initial linear trends of the normalized extreme depth of failure $d_f^e/a$ for $SL \leq 1$ is defined by:

$$\frac{d_f^e}{a} = 1.25 \cdot SL - 0.51 \pm 0.1 \qquad (8)$$

The extreme depth of failure increases at a lesser slope of 0.75 to a maximum at $SL$ = 1.5.

The range for the mean depth of failure $d_f^m$, including locations with no failure, was established by calibrated numerical modeling by Perras & Diederichs (2016) (see Kaiser (2016c)). It typically ranges between 20 to 30% of $d_f^e$:

$$d_f^m \approx \frac{d_f^e}{3.5 \text{ to } 4.5} \qquad (9)$$

Based on these semi-empirical relations, it is possible to anticipate the mean and extreme depths of failure in brittle failing rock.

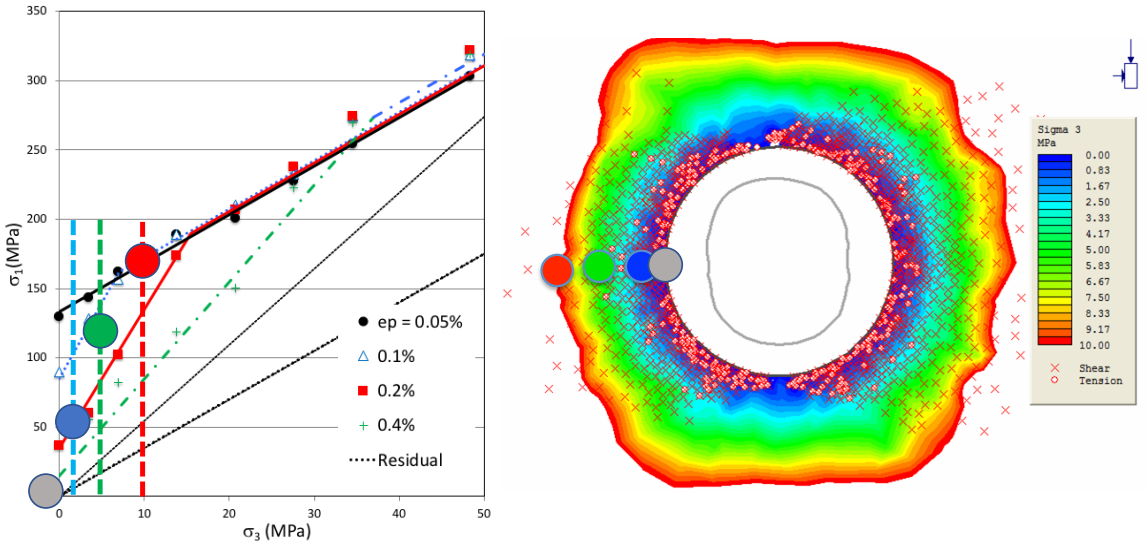


(a) (b)

Figure 11 (a) Illustration of four states at locations indicated by circles in principal stress space for Marble (Fig. 9); and (b) continuum model of tunnel showing yield locations (x for shear and o for extension) for $k_o$ = 0.5 together with confining stress $\sigma_3$ contours.

*Depth of strainbursting $d_{SB}$*

The depth of strainbursting is difficult to predict because instability not only depends on stress and strength but on stress gradients and geometric factors, too. It can be as little as the depth of an

individual spall or as deep as the extent of highly stressed rock. Strainbursts occur at locations of stress raisers as illustrated by the principal stress contours in Figure 6. These stress raisers occur at the outer limit of the inner shell and can easily involve 25 to 35% of the tunnel radius (e.g. 0.75 to 1 m for a tunnel with a radius $a$ = 3 m).

By reference to Eqns 8 and 9, it can be argued that the depth of strainbursting falls somewhere between $d_f^m$ and $d_f^e$; i.e. for $d_f^m$ = 1/4 $d_f^m$, $d_{SB}$ = 0 to 3/4 $d_f^e$ (e.g. between 0 and ≤ 1.65 m for $a$ = 3 m and $SL \leq 1$). In gradually spalling ground, $d_{SB}$ is near zero and for typical tunnel sizes in massive to moderately (unfavorably) jointed ground $d_{SB}$-values of 1 to < 2 m must be expected. This is consistent with observations from strainburst-prone mines. The total depth of failure after a strainburst, may be larger as some burden may be ejected and blocky ground may unravel after the burst.

### 3.2.4 *Geometric bulking of stress-fractured rock*

Stress-fractured and bursting ground bulks when deformed past the peak strength of the rock mass. This leads to unidirectional bulking deformations that are controlled by the excavation geometry and the imposed tangential strain (Fig. 12a). This directional bulking process is not captured by dilation models that relate the strength to the volumetric strain (bottom of Fig. 12a).

*Estimation of geometric bulking displacement at wall*

The geometric bulking deformation can be estimated following the semi-empirical approach outlined by Kaiser (2016c) whereby the estimated depth of failure $d_f$ (not $d_y$) is multiplied by a confining pressure dependent bulking factor $BF(\sigma_3)$ (Fig. 12b). In bursting ground, pre-burst fracturing to $d_f$ imposes a wall displacement $d_f$ *$BF_{static}$ on the support and the strainburst adds further displacements $d_{SB}$*$BF_{SB}$ (note: $BF_{static}$ and $BF_{SB}$ are not necessarily equal). For example, at an average confining pressure $\sigma_3$ = 0.1 MPa, excavation-induced bulking is estimated at $BF$ = 3%. For $a$ = 3 m and $SL$ = 0.8, a depth of failure of $d_f$ = 1.47 m causes $d_{wall}$ = 44 mm. This displacement consumes some of the displacement capacity of the installed support before a potential burst.

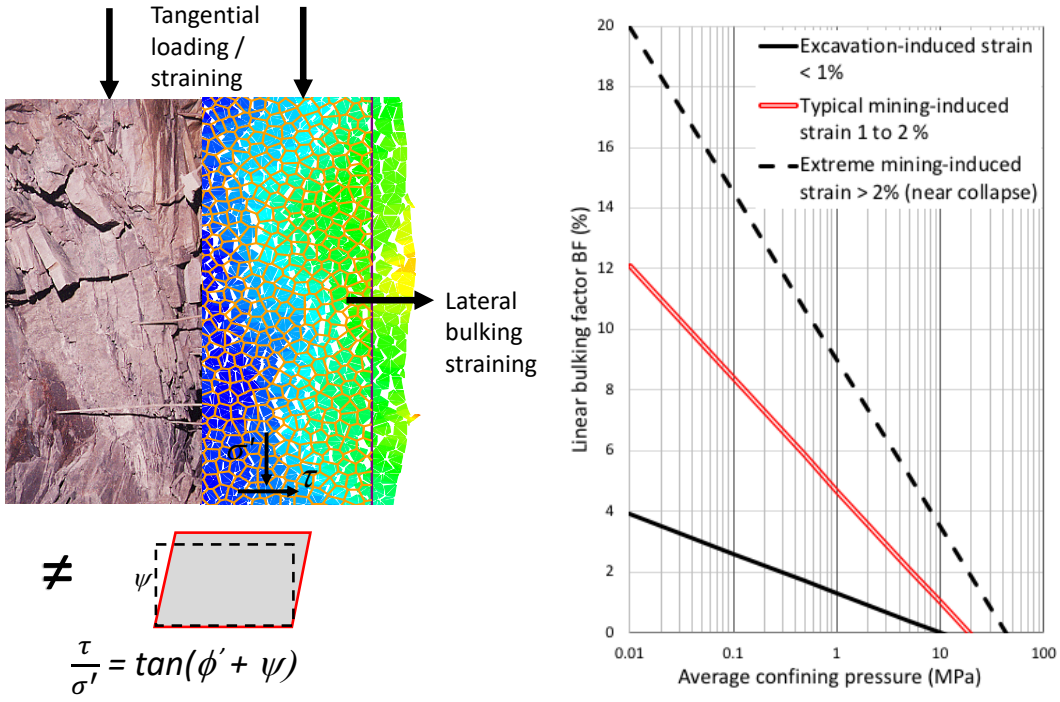


(a) (b)

Figure 12 (a) Unidirectional rock masses bulking due to stress-fracturing (photo) reflected in cartoon-like Voronoi model ≠ non-representative dilation model; and (b) semi-empirical bulking factor charts (modified from Kaiser 2016c) for excavation and mining-induced bulking.

The mining-induced bulking is larger because of the increased geometric non-fit at larger deformations. For a mining-induced or strainburst associated strain of 1 to 2% the chart indicates a bulking factor $BF$ = 8%. Hence, a strainburst of $d_{SB}$ = 1 m would add 80 mm. If the support does not have a

remnant displacement capacity of 80 mm, it will fail. The total displacement after the burst will be 124 mm.

*From common to best practice*

Again, there are ample opportunities and economic, as well as safety benefits, that can be derived from differentiating between near wall (inner shell) and outer shell behaviors. This is particularly valid for support designs where bulking deformations from statically and dynamically deformed stress-fractured rock dominate the rock mass behavior.

Different EDPs dominate the behavior in the inner and outer shell. Separate EDP-value sets need to be defined to assess the vulnerability to damage and the fragility in order to select appropriate rock support systems.

## 4 ROCK MASS CHARACTERIZATION

"Den Werkstoff Fels in seinem Zustande und seinem Verhalten zu beschreiben, ist die erste Aufgabe dessen, der seine Felsbauwerke sicher anlegen, zweckmäßig konstruieren, schön gestalten und wirtschaftlich ausführen möchte." or "Describing the construction material, the rock mass, in its condition and its behavior is the first task … to safely lay out, sensibly construct, …, and economically execute works in rock." (Müller 1963)

For this purpose, the goals of rock mass characterization have to be tailored to the technical objectives of an investigation. For example, for cave engineering, the workflow includes the assessment of five engineering aspects (Brown, 2007): caveability; fragmentation; cave performance; extraction level stability; and mine construction (rock support). Each has to address specific questions and each design component is influenced by a different rock mass behavior and thus is dominated by different rock mass properties. For example, the vulnerability to stress fracturing (spalling), the bulking characteristics for flow control and support selections, and the confining stress impacts on pillars or support design are dominated by different EDPs. As discussed previously, the development of best practices in rock mass characterization therefore starts with the identification of critical EDPs including related rock mass characteristics and properties.

In underground construction, the rock mass has to be described long before access to observe its behavior is possible. This demands a systematic approach of rock mass quality quantification moving from 'inferred' to 'proven' rock mass quality (Section 4.1), a practice that is often ignored or rarely systematically executed.

With increasing depth, the changing rock mass behavior creates additional challenges for the mining engineer. At depth, the rock is highly stressed, closer to failure, and often more confined leading to a higher interlocking and elevated strength. This issue is covered in Section 5 on rock mass strength estimation.

An effective rock mass characterization program, including logging, mapping and laboratory testing, needs to collect and interpret features that are relevant for clearly defined purposes. How to overcome challenges of rock mass characterization for underground construction in deep mining is covered by Kaiser et al. (2015). The recommended methodology is not repeated here.

In the following, two aspects are addressed to assist in the application of best practices in rock mass characterization: (1) stages of characterization to move from 'inferred' to 'proven' quality descriptors, and (2) the suitability of classifications for rock mass characterization.

### 4.1 *Stages of rock mass characterization – from assumption to fact*

Rock mass characterization involves many model-building components: geological, structural, rock mass, and hydro-geological models. These models are being developed in an incremental and iterative manner with data initially collected during scoping studies from boreholes. The data is then gradually refined during follow-up studies and eventually during the construction phases by mapping and back-analyses of monitoring results. What is often ignored in common practice is to clearly define and register assumptions such that the characterization program can focus on eliminating one assumption after another and on replacing them with factual, reliable information.

As for mineral resource definition increased knowledge and confidence needs to be built from 'inferred' to 'indicated' to 'measured' or from 'inferred' to 'probable' to 'proven' (on left of Fig.13).

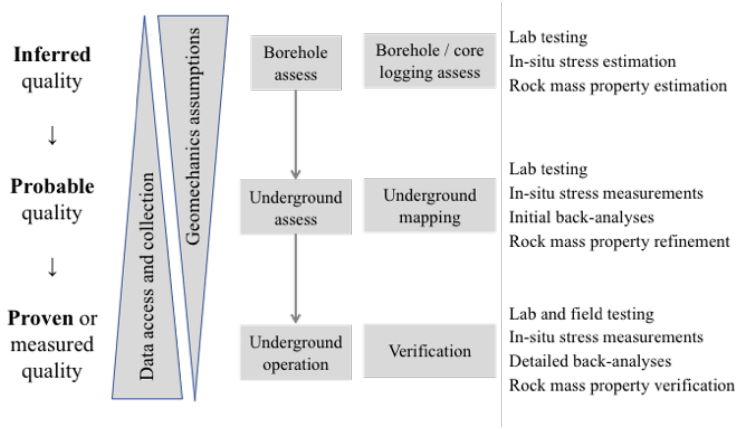


Figure 13 Evolution of data collection to eliminate or confirm geomechanics assumptions at different stages of a rock mass characterization program.

Assumptions have to be made in the early stages of a characterization program, assumptions that are inferred from comparable rock formations and existing empirical rules from similar rock masses. Next, uncertainty has to be incrementally removed by reducing the variability and move toward 'probable' data. For this purpose, targeted data collection focused on specific assumptions is to be used and documented to ensure the credibility of information. Finally, assumptions can be removed and replaced by 'measured' data or 'proven' quality ratings when sufficient factual data is available (likely after underground observations are available). Some assumptions may never reach the status of 'measured', e.g. in-situ stress, and back-analyses of other monitoring data may be required to reach the 'proven' class. This approach is illustrated by the wedges in Figure 13.

The use of qualified professionals to make necessary assumptions is a very important principle of geotechnical engineering as it is better to extrapolate from experiences and to plan based on comparable information. However, boundaries between assumed and measured (or proven) information are often blurred and it is essential to clearly define and then replace assumptions by facts as the site characterization proceeds. Eventually, the validity of all assumptions has to be proven.

Best practice in rock mass characterization includes a registry of assumed EDPs (incl. their variability) and tracks the path from assumption to fact. While EDP-values have to be inferred during the preliminary design phase, good engineering practice demands that they are raised to probable and then to a proven status with minimal remnant uncertainty.

### 4.2 *Characterization versus classification*

Ideally, a rock mass is characterized in a comprehensive manner such that all engineering questions can be answered. However, because different engineering tasks require different EDPs, most rock mass classification systems focus on one or two applications (e.g. support selection). Strictly speaking only part of the classification deals with the characterization of the rock mass (block size and interlock, condition and persistence of joints, etc.), the remainder deals with the application for a defined purpose (support selection, rock mass strength determination, etc.). For this reason, and because of the fact that each classification system considers different parameters and assigns different weights, specific classification indices (Q, RMR, MRMR, GSI, etc.) should not be correlated. They should be used independently for the purposes defined by the developers and for the ground conditions that form the foundation for the classification system.

Even the GSI (Geological Strength Index), while not providing guidance for support selection, was developed with a bias toward the characterization of a rock mass in the low confinement range near excavations (slopes or inner shell of tunnels). Furthermore, the GSI was introduced for collecting field information for rock mass strength determination and "to address two principal factors considered to have important influences on the mechanical properties of a rock mass, i.e., the structure (or blockiness) and the condition of the joints" (Hoek & Brown, 2019). Strictly speaking, the GSI-system was developed only for rock mass strength estimation and for conditions of blocky ground (see Section 5).

While each classification system stands on its own merit, the indiscriminate use of rock mass classification without consideration of the limit of applicability obtained from the implicit data sources and

without respect for the types of engineering projects (slopes, tunnels, mining (pillars and caves)) has led to serious consequences and is strongly discouraged.

For example, conventional rating systems such as RMR, Q and GSI were developed and calibrated for conditions not dominated by large mining-induced stress changes and stress-fracturing of strong rock blocks. Hence, they are often not applicable, for example, for defected rock and in large strain environments. If the GSI is indiscriminately applied to conditions other than those used to develop the GSI-based strength equations, the resulting rock mass strength tends to be underestimated (see Section 5).

Other deficiencies of rock mass rating systems are addressed in more detail in the ISRM on-line lecture on "Challenges of Rock Mass Strength Determination" (Kaiser 2016a) and the impact of rock mass heterogeneity on in-situ stress variability is discussed by Kaiser (2016b).

Furthermore, because of the common practice of collecting rock mass classification data without having identified the controlling EDPs and without following an 'assume, revise and verify' approach to move from 'inferred' to 'proven' status (Fig. 13), excessively detailed information is often collected and then not distilled to the essentials. More importantly, properties that may dominate the behavior of the rock mass are ignored (e.g. tensile strength to anticipate spalling or rock fragmentation).

Following the rationale outlined in this article, it is of primary importance to identify whether a rock mass belongs to one of three classes (RMQ1 to 3; refer to Figs. 4 and 5). This is particular significant when estimating the rock mass strength (Section 5).

*From common to best practice*

Again, opportunities and economic as well as safety benefits can be derived by moving from common to best practices in rock mass characterization. Too many parameters are frequently collected that, in the end, do not matter, and essential parameters are ignored or only collected late in a project when unexpected rock mass qualities (changed conditions) are encountered.

Targeted rock mass characterization should be guided by identified EDPs and by the eventual intent (engineering tasks). For example, the Q-system was originally intended for support selection and then expanded for TBM and other applications, whereas the GSI-system was developed for rock mass strength determination. Both should be used with discretion for the intended purposes. Most importantly, they should be used to identify RMQ-classes that matter for the performance of underground excavations (RMQ1 to 3). The influence of stress (and water) should be treated separately at the characterization stage and only considered when used for engineering designs. Limits of applicability need to be respected (see Section 5 for GSI).

Best practice in rock mass characterization has to follow a systematic process to move from inferred to proven rock mass quality designations. Many 'unexpected' problems could be anticipated if the full spectrum of possible ground conditions was properly described by clarifying inferred from probable and proven conditions. In this manner, claims for 'changed conditions' can be prevented because construction techniques suitable for uncertain conditions can be selected.

Similarly, the development of in-situ testing and monitoring programs should focus on critical components of the path from assumption to fact.

## 5 ROCK MASS STRENGTH ESTIMATION

Some of the challenges in rock mass strength estimation for the design of deep underground excavations are covered by Kaiser (2016a) building on the work by Bewick et al. (2015) and Kaiser et al. (2015). More recently, the GSI-approach has been 'updated' not because fundamental changes were required, but to "discuss many of the issues of its utilization and to present case histories to demonstrate practical applications ..." (Hoek & Brown, 2019). In a companion paper Bewick et al. (2019) provide guidance for rock mass strength estimation when the limitations of the GSI-strength equations are reached.

"Why do we tend to underestimate the rock mass strength for underground construction at depth?" was the lead question raised during the ISRM lecture. The basic answer is that common practices fail to capture the strengthening effect of interlock in non-persistently jointed rock where failure through intact rock adds strength, and geometric bulking leads to a more rapid strength gain at elevated confining stress. As outlined in detail in the on-line lecture, best practice in rock mass strength determination certainly does not always follow common practice.

For situations where blocks exist (blocky ground with three persistent joint sets) and block rotation is possible (even if interlocked to some extent), Hoek & Brown (1997 and 2019) present GSI-based strength equations for isotropic rock masses containing block forming joints and blocks without defects. They indicate that the underlying GSI-experience stems from excavations in rock masses where block rotation contributes to the failure process. The following GSI-strength equations are therefore valid for RMQ2 and 3:

$$\sigma_1' = \sigma_3' + \sigma_{ci}'(m_b \frac{\sigma_3'}{\sigma_{ci}'} + s)^a \qquad (10)$$

where, $m_b = m_i exp\left(\frac{GSI-100}{24}\right)$; $s = exp\left(\frac{GSI-100}{9}\right)$, and $a = \frac{1}{2} + \frac{1}{6}(e^{\frac{-GSI}{15}} - e^{\frac{-20}{3}})$.

However, if rock blocks are strongly interlocked and block rotation is restricted, the rock mass will be able to mobilize extra strength, particularly when it is highly confined ($\sigma_3 > UCS/10$). As illustrated by Figure 14a, the rock mass strength, extrapolated using Eqn 10, from low to high confinements can be as low as 50% of the anticipated confined rock strength with interlocked and shear rupture behavior (compare black to red arrow at $\sigma_3$ = 20 MPa). The shaded area in Figure 14a illustrates the difference in strength obtained by extrapolation from inner shell values.

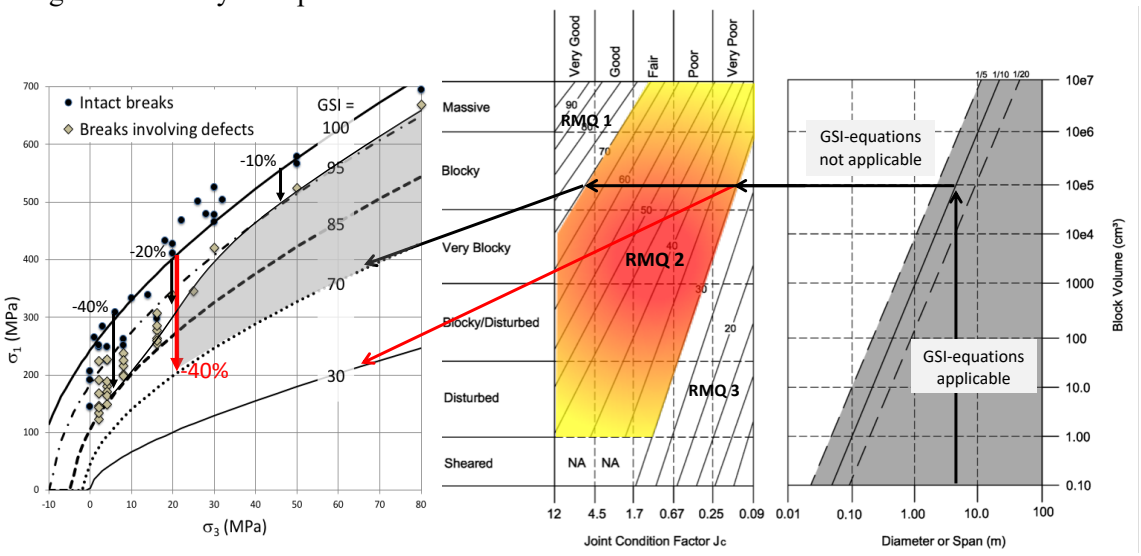


Figure 14 (a) Example of strength degradation and underestimation by GSI-strength equations; (b) applicability range for RMQ2 boundaries; and (c) scale applicability limits for GSI-strength equations.

When Eqn (10) is adopted, it is implicitly assumed that the degree of interlock is sufficiently small such that the rock blocks formed by open joints can rotate during the failure process. In massive to moderately jointed rock this is not the case and the strength is controlled by stress-fracturing of rock blocks, rock bridges and asperities, and by the dilation of highly interlocked rock fragments. Hence, the strength degradation from the intact rock strength is much less at elevated confining pressures than conventionally assumed (Bahrani et al. 2013 and 2016). Consequently, the rock mass is much stronger than anticipated by the standard models as elaborated by Kaiser (2016a) and illustrated by Figure 14a.

### 5.1.1 *Applicability limits of GSI strength equations*

At depth, the rock mass is often massive to moderately jointed with non-persistent joints and joints are highly compressed leading to further strengthening effects due to 'over-closure' (Barton et al. 1985). Consequently, the conventional GSI-strength equations are rarely applicable for RMQ1, not even for RMQ2 at high $J_c$-values (Fig. 14c) when the rock mass is highly confined as encountered at depth. Similar deficiencies have to be overcome when rock mass classifications are used for the design of excavations at depth.

There is another basic assumption of the GSI approach that needs to be respected, i.e. it is only applicable for rock masses that can be assumed to be isotropic and simplified to a continuum, i.e., if the block volume is small relative to the excavation size. For common engineering problem scales, the

GSI-strength equations are applicable when a rock mass is made up of blocks with edge lengths smaller than 1/10 (range 1/5 to 1/20) of the problem dimension (i.e., tunnel diameter, excavation span and pillar height). Based on this criterion, the applicability of the GSI-strength equations can be assessed using Figure 14c.

They are applicable for:

- shafts or raises of 1 to 4 m diameter for very blocky to sheared ground with block size < $10^4$ to $10^5$ cm$^3$;
- standard tunnel sizes and pillar heights (5 to 10 m) for blocky ground with block size < 1 m$^3$; and
- large caverns and caves (span > 20 m) as long as the persistence of joints in very strong rock is sufficient to create non-interlocked blocks in the 10 to 1000 m$^3$ range.

For example for a 5 m wide tunnel, GSI-equations can be used for very blocky or worse ground (as indicated by arrow in Fig. 14c).

As mentioned previously, Bewick et al. (2019) provide guidance for rock mass strength estimation when the limitations of the GSI-strength equations are reached. It is not that the GSI is not applicable, as erroneously implied by the wording in previous publications by the author (e.g., by mentioning the GSI applicability limits in the ISRM on-line lecture), but the applicability of the GSI-strength equations is limited.

*From common to best practice*

The common practice of indiscriminate use of the GSI-strength equations (Eqn 10) for rock masses of RMQ1 and part of RMQ2 tends to underestimate the strength. They are applicable for 'soil like' behavior in RMQ3 for failure mode $M_{32}$ and $M_{33}$, and for RMQ2 of very blocky ground with low $J_c$-values. For massive to moderately jointed rock masses with GSI > 65, the systematic methodology for estimating equivalent rock mass strength parameters, outlined by Bewick et al. (2019), should be adopted. This methodology compliments the HB-GSI approach for rock mass strength estimation of a massive to moderately jointed rock mass.

The best practice to obtain reliable rock mass strength include the elements explained by Kaiser et al. (2015). Because best practice approaches must overcome the deficiency of common practices that tend to underestimate confined strength of highly stressed rock, it is advisable to adopt an observational approach, starting with experience-based, inferred assumptions, replacing them increasingly with verified, proven facts.

## 6 GROUND CONTROL – SUPPORT SELECTION

### 6.1 *Introduction*

Various rock mass classification systems (e.g., Q, RMR, etc.) have found wide application for support selection. These approaches are suitable if conditions at a project match those that form the underlying classification databases, i.e. civil tunneling data. They may however not be suitable when conditions change as they do in mining applications where stresses and failure modes change, or when the rock mass behavior at great depth differs. Unfortunately, rock mass classifications are frequently applied beyond their range of applicability. For example, they may be applicable for the advance of mining tunnels during mine development but are inapplicable when mining-induced stress changes dominate the excavation and support behavior.

Whether a support is selected based on risk or on a more conventional factor of safety-based design approach, load, displacement, and energy demands are compared with respective support system capacities. For static conditions, the support design is commonly dominated by load equilibrium (wedge stability) or displacement compatibility (squeezing ground) considerations (Eqns 1 & 2). For dynamic earthquake or rockburst loading, it may be necessary to also consider energy equilibrium conditions (Eqn 3). It is therefore mandatory to estimate three demands (load, displacement and energy) and the capacity of the integrated support system.

One important step in rock support design is to identify potential failure modes as explained in Sections 2. Only when the anticipated failure modes are correctly identified, can the most appropriate methods for demand estimation be applied.

In each design domain, the load, displacement and energy demands on the rock support are calculated individually by considering all possible excavation damage mechanisms. This is achieved by evaluating the damage severity in terms of depth of failure, rock mass bulking, and the anticipated

impact velocity (if applicable). It is often difficult to know in advance which type of damage mechanism will eventually dominate. Hence, it is advisable to analyze all reasonably possible damage mechanisms and then identify the critical support demands, i.e., the possible worst-case scenario.

Once the demands on the support are identified, it can be evaluated whether a rock support system can be designed to control the failure process. If excessive demands are identified, other means of ground control management such as destressing, hydro-fracturing, etc., may have to be deployed to help reduce the support demand.

#### 6.1.1 *Capacity estimation*

The load, displacement, and energy capacities of individual support components (mesh and shotcrete, or bolts and cable bolts) are conventionally obtained from pull-out (direct loading) or split tube (indirect loading) tests in the laboratory or in the field. Respective component capacity data are available from the literature (e.g. Cai & Kaiser, 2018) or site-specific values are obtained from field tests.

Unfortunately, these test results are highly dependent on the adopted test method and the ability of the support to resist internal loading is often unknown. Furthermore, the ultimate capacities reported in the literature may in practice not be reached (e.g. due to operational constraints such as allowable convergence) and, most importantly, the respective ultimate capacities are not simultaneously reached. A methodology to establish the capacity of integrated support systems utilizing all individual support components is discussed in Section 6.2).

#### 6.1.2 *Demand estimation*

Load demands are obtained by estimating the volume of anticipated unstable ground (wedges, volumes or depth of stress-fractured ground) and by assessing the remnant load capacity after accounting for the simultaneously available bolt and surface support capacities. For dynamic conditions, the shakedown potential is established by adding a dynamic acceleration to the gravitational acceleration.

Displacement demands are commonly obtained by the use of analytical models (ground-reaction curves) or continuum numerical models with non-linear constitutive models. Both models are deficient when geometric bulking of stress-fractured ground in the inner shell of the excavation dominates the displacement demand. As a consequence, commonly adopted capacity models to represent individual support components are often limited in that the interaction between rock support and rock, particularly stress-fractured rock, is not fully captured; i.e. the displacement demands imposed by the fractured rock are underestimated.

Energy considerations are adopted when kinetic energy demands from earthquakes or rockbursts are anticipated. Unfortunately, energy cannot be measured rendering the energy-based designs unverifiable. However, because the product of displacements times bolt forces defines the energy consumption of a support component and the integrated support system, displacements provide an indirect measure of the energy consumed by the support system. It is for this reason that a deformation-based support design approach was introduced by Kaiser (2014) (discussed further in Sections 6.4). Displacement-based designs have a major advantage in that both displacement demands and capacities can be measured and compared with model outputs and field measurements of displacements (e.g. from laser surveys).

### 6.2 *Support system capacity (SSC) estimation*

An integrated support system is made-up of compatible support components (bolts, cable bolts, mesh, shotcrete, etc.) with load–displacement characteristics of individual support components obtained from static or dynamic laboratory or field tests. These components have to work together (in parallel) to provide rock retention, reinforcement, and holding functions (Cai & Kaiser, 2018). The capacity of each component is first mobilized and then consumed until it fails. The impact of the installation sequence on the differential loading or straining of support components has to be considered and all possible weak links in the rock support system have to be eliminated.

Much effort has been expended around the world to establish direct and indirect load, displacement, and energy dissipation capacities of support components. However, there is no systematic engineering approach to estimate the capacity of the integrated support system consisting of a bolting and surface support system.

A means to estimate the direct and indirect load capacities is introduced for direct loading by Cai & Kaiser (2018 in Chapter 4) and expanded for direct and indirect loading by Kaiser & Cai, (2019 in

Chapter 3). For this purpose, it is assumed that all bolts work in parallel, meaning that they are simultaneously loaded at the plate through a surface support system (direct loading) and strained along the bolt by the relative movement of fractured rock blocks (indirect loading). For the prototype model, the load–displacement characteristics of individual support components are approximated by an equivalent perfectly plastic model (Fig.15a) to generate the cumulative support system load profile (Fig.15b). The corresponding displacement and energy dissipation profile of the support system is presented in Figure 16.

The support system's displacement capacity can be expressed as $\delta_{system} = \delta_{bolt\ (direct\ and\ indirect)} + \delta_{surface}$, where $\delta_{bolt}$ represents the bolt's displacement capacity (with the most deformable bolt controlling the maximum capacity) and $\delta_{surface}$ the surface support's displacement capacity. The static or dynamic energy capacity of the support system $E_{system} = \Sigma E_{bolt\ (direct\ and\ indirect)} + E_{surface}$, with $\Sigma E_{bolt}$ represents the cumulative energy capacity of all installed bolts at a given mining-induced displacement $\delta_{bolt\ plate}$, and $E_{surface}$ represents the surface support's energy capacity at a given bolt plate displacement. This approach greatly differs from commonly adopted approaches in that the energy sharing between support components is accounted for and the deformation compatibility for the entire rock support system is respected. The self-supporting capacity of the reinforced stress-fractured rock mass is ignored in the prototype model described in the following sections.

### 6.2.1 *Load capacity of support systems*

The load capacity of a support system, obtained by superposing individual support component capacity-displacement characteristics, is illustrated by Figure 15b for a support system consisting of two support components (rebar and cable bolts) with an assumed elasto-plastic load–displacement characteristic. Figure 15a shows various approximations of actual pull test data for direct loading by an equivalent plastic load–displacement characteristic, i.e., a mean load (force) capacity $F_m$ and an ultimate displacement capacity of individual bolts $\delta_{ult(B)}$.

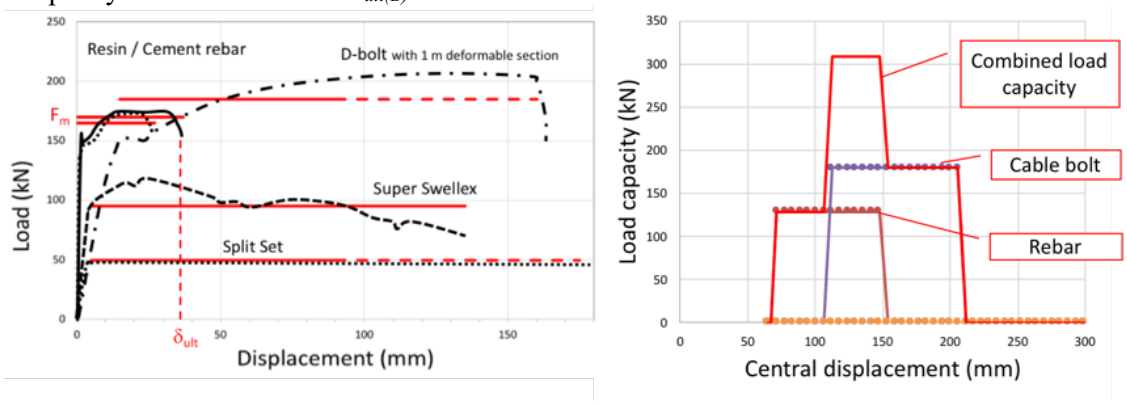


(a) (b)

Figure 15 (b) Approximation approach for various directly loaded bolt types, and (b) Load capacity of a support system consisting of two plastic support components (180 kN rebar and 250 kN cable at 1.2 m spacing) with mesh over mesh-reinforced shotcrete.

Note: the dashed sections in Figure 15a indicate that the ultimate displacement capacity obtained by pull-out tests may not be available for Split Set bolts that are resisting over an anchor length measuring less than the test length. Furthermore, if test data are derived from indirect or split tube tests much less displacement capacity will be available for directly loading as indicated for the D-bolt.

### 6.2.2 *Energy and displacement capacity of support systems*

The energy capacity of a support system depends on the imposed displacement. This is illustrated for the same two-component support system of sequentially installed bolts loaded via mesh-reinforced shotcrete by Figure 16a. The bolts in this support system are activated after 65 mm of central deflection and the support system fails at 200 mm when the cable bolt reaches its ultimate displacement capacity.

Figure 16b also shows the decreasing remnant support capacity that is available as the support is deformed. These figures illustrate a most relevant interdependence of energy and displacement capacities.

### 6.2.3 *Support system capacity consumption (SSCC)*

The effectiveness of support systems can be compromised by quality deterioration (e.g., corrosion; not covered here) and by the consumption of a support system's displacement and energy capacity. Mining not only causes stress changes but also produces associated deformations and tunnel convergence which deform and strain the support. As these displacements increase, part of a support's displacement and energy dissipation capacity gets consumed. This is called support capacity consumption and is reflected in the support energy consumption plot (shown in red in Fig.16b). The support system capacity for this illustrative example is gradually lost until all of its capacity is consumed at 200 mm imposed central displacement. At 150 mm central displacement only 8 kJ/m$^2$ or 40% energy capacity remains.

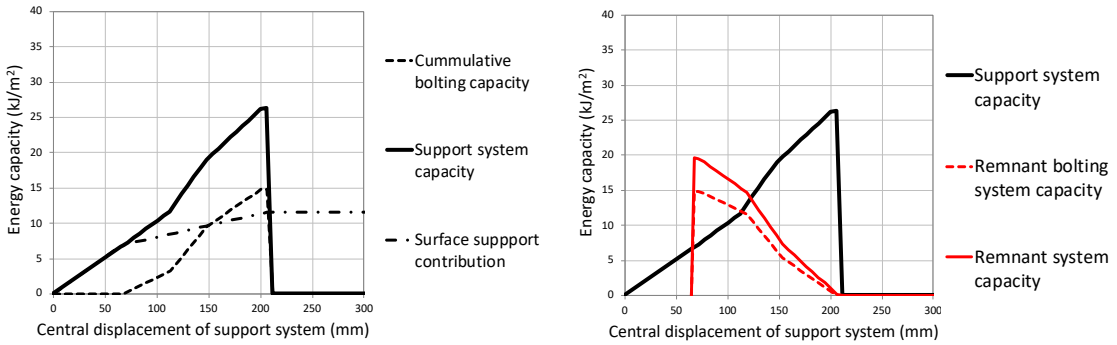


(a) (b)

Figure 16 (a) Energy–displacement characteristics of the same support system as in Figure 15, loaded via a mesh-reinforced shotcrete surface support, and (b) remnant capacity (red) as a function of applied displacement (central deflection between bolts); 'Central displacement' refers to the maximum displacement at the mid-span between bolts).

As schematically illustrated by Figure 17, if an installed support system is deformed to a wall deformation $\delta_1$, the support system has reached its yield load capacity and its elastic energy capacity $E_1$ has been consumed. The remnant displacement capacity to the first point of the support system degradation at $\delta_3$ is $(\delta_3 - \delta_1)$ or the remnant energy capacity is reduced to $(E_2 + E_3)$. Then, if during mining the support is further deformed to $\delta_2$, the remnant displacement capacity drops to $(\delta_3 - \delta_2)$, and the corresponding remnant energy capacity is reduced to $E_3$. In this manner, the support capacity is consumed as it is deformed.

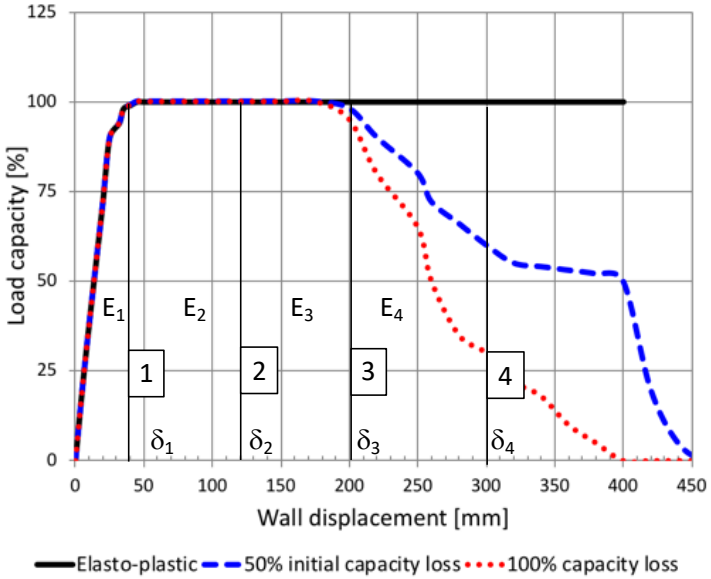


Figure 17 Schematic support system characteristics illustrating four stages of support capacity consumption [1] to [4]. Energy $E_1$ is the energy used to deform the support from 0 to $\delta_1$, $E_2$ from $\delta_1$ to $\delta_2$, etc. The load capacity is defined as a percentage of the peak load capacity (Cai & Kaiser, 2018).

At the displacement $\delta_3$, the support system starts to lose its load capacity. Two degradation scenarios are shown in Figure 17 by the dashed and dotted support degradation curves. The system still has some load and displacement capacities but the remnant energy capacity, i.e. the area under these curves, rapidly drops. For this reason and for design purposes, the displacement capacity $\delta_3$ is defined as the 'allowable' displacement capacity of the support system.

This example illustrates how the support system capacity is being consumed by mining-induced displacements, i.e. by displacements imposed in a static or gradual manner, or by co-seismic deformations in seismically active mines (Kaiser 2017). How to recognize support consumption in the field is discussed in Section 6.2.5.

The practical implication of the support system capacity consumption is that a support system rarely exhibits its full capacity that was available at the time of support installation.

*Consumption of retention system capacity*

Similarly, the energy capacity of retention systems can be consumed as they are deformed. According to Figure 18, chain-link mesh could have a capacity of 10 to 13 kJ/m$^2$ but only if >300 mm central deflection is acceptable. Because bagging between bolts must be limited for operational reasons and to minimize bending of bolt heads, it is advisable to design for allowable rather than ultimate capacities. For example, at 100 to 200 mm central deflection $E_{100}$ to $E_{200}$ represents a meaningful, allowable energy design capacity (red boxes in Fig.18).

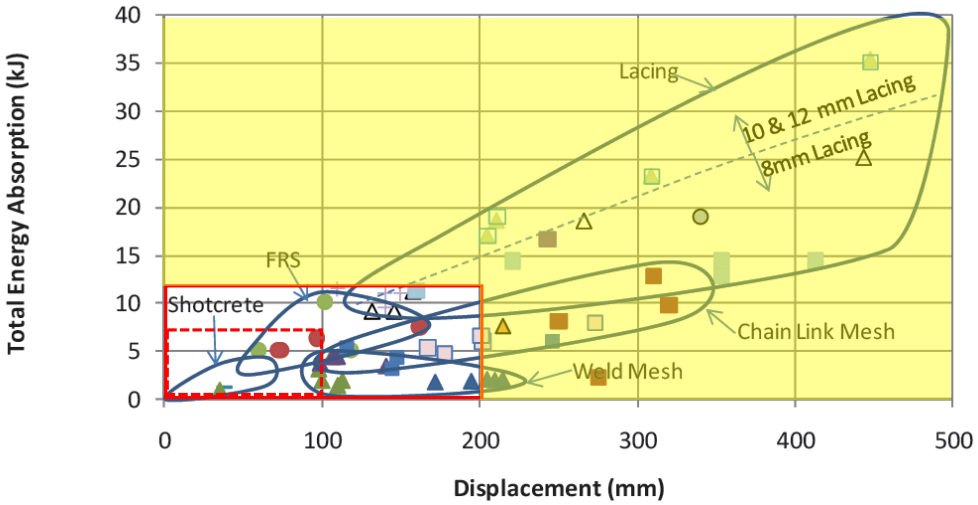


Figure 18 Total energy absorption capacities of retention systems showing ranges of acceptable retention system performance at 100 to 200 mm allowable central deflection (modified after Potvin et al. 2010).

By analogue, if the capacity of a support system can be consumed, it must be possible to restore its capacity by installing additional support after displacements have been imposed on the support. This is called 'proactive or preventive support maintenance' (PSM). This introduces an important support design scenario for situations where the support capacity is lost with 'time'.

### 6.2.4 *Support system capacity restoration by proactive support maintenance (PSM)*

Once some support capacity has been consumed, the support capacity can be restored by adding bolts offering an extra displacement capacity. By reference to Figure 17, the ultimate displacement capacity may be increased from the ultimate displacement capacity of the support system ($\delta_{ult(SS)} = \delta_3$) to $\delta_4$ or more. For example, if a PSM was conducted at $\delta_2$ to increase $\delta_{ult(SS)}$ to $\delta_4$, the remnant energy capacity would increase from $E_3$ to ($E_3 + E_4$) with $E_4$ represented by the area under the full load capacity. The remnant energy capacity would double.

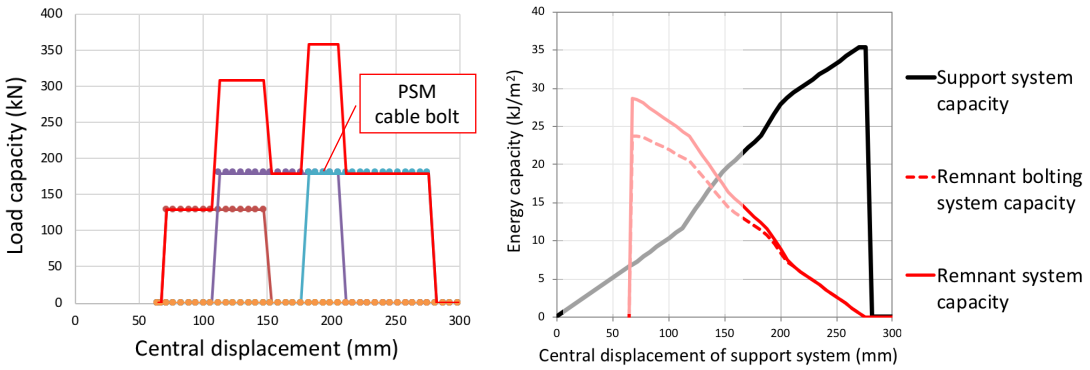


(a) (b)

Figure 19 (a) Load capacity after PSM with 250 kN cablebolts at 70 mm bolt head or 170 mm central deflection, and (b) combined capacity and remnant capacity after PSM for comparison with Figure 16b.

If the two-bolt system (rebar and cable bolts) presented in Figure 15b is enhanced by adding cablebolts at a spacing of $s$ = 1.2 m after a bolt head displacement of 70 mm or a central displacement of 170 mm, the load capacity line extends to 280 mm (Fig.19a), and the energy capacity increases from 26 to 35 kN/m$^2$ (compare Fig.16a and 19b). The remnant capacity line is shifted upward by 9 kJ/m$^2$. Hence, both the remnant displacement and the energy capacities of the support system at 70 mm have increased by a factor of more than 3, i.e. if extra cable bolts were installed at a central displacement of 170 mm.

### 6.2.5 *Visual recognition of SSCC for implementation of PSM*

Figure 20 demonstrates the concept of the support capacity consumption with photos illustrating increasing support damage (and support capacity consumption) toward the location where the support failed and the excavation collapsed (at the back end of the drift). The displacement scale in the load–displacement graph depends on the composition of the integrated support system.

Displacement ranges are superimposed by arrows to indicate where the original or the baseline design is valid (e.g. to the displacement limit at 100 mm) and when proactive support maintenance is needed or is most effective (e.g. between 80 and 180 mm). If the opportunity is missed to proactively enhance the support, failure may occur and rehabilitation[6] will be required to prevent collapse. The photos illustrate how the support system consumption is reflected by an increasing support damage.

Proactive support maintenance is a practical and often an economical means to increase workplace safety and reduce the potential severity of excavation damage. PSM is particularly beneficial when unexpected large convergences are encountered (measured) as it allows for focused PSM. This may offer an economic alternative to installing burst-resistant or yielding support systems across the board, particularly when high support demand is localized and the locations requiring such a support are not a priori foreseeable.

Deformation-based support selection and PSM procedures can be developed utilizing mine-specific convergence measurement data. With recent improvements in the speed of digital convergence monitoring, PSM can be deployed in a cost-effective manner.

[6] It is important to distinguish between support 'maintenance' and 'rehabilitation'. Support maintenance means that the support is upgraded to 'maintain' a sufficient capacity during future loading episodes. Support rehabilitation implies that the support was damaged to the point where it has to be replaced to 'restore' the original support capacity.

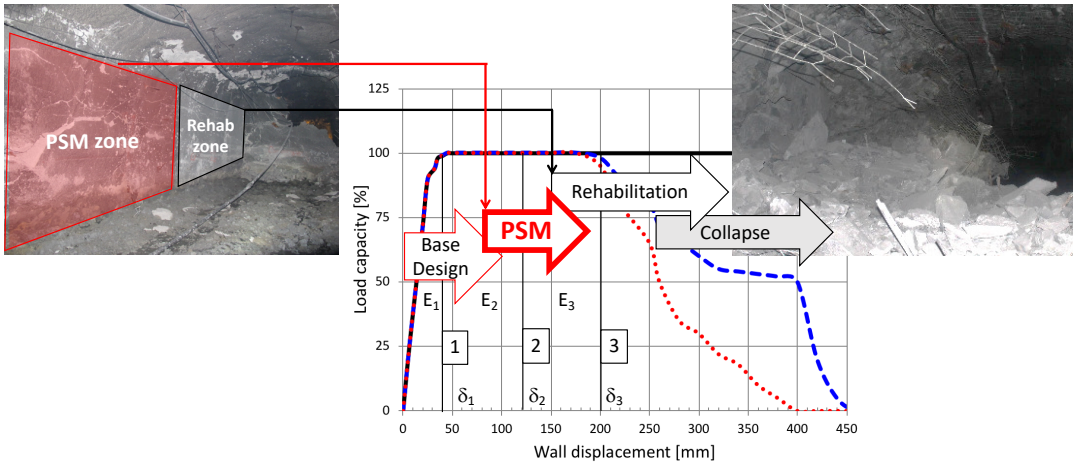


Figure 20 Illustration of support system capacity consumption and range of applicability of base design, proactive support maintenance (PSM) and support rehabilitation (Photos courtesy: Deep Mill Mining Zone at Grasberg Mine, PT Freeport Indonesia 2017).

### 6.2.6 *Safety margin and damage limits of integrated support systems*

Based on previous considerations of support capacity consumption and remnant support capacity, it is meaningful to define the safety margin in terms of remnant capacity. The safety margin can be defined with regard to displacement and energy or a combination of both. In Figure 21, the remnant capacity at FS = 1 is shown in red and for a $FS_{Disp}$ = 1.3 is displayed by the green full line. When this line is reached, the support system has a remnant displacement capacity of 23% of the original displacement capacity at a given energy demand level.

In practice, damage levels (e.g. R1 to R5 (Cai & Kaiser, 2018)) are frequently used to assess the status of a damaged support system. When displacements reach the remnant capacity, increasing signs of support deterioration are to be expected (e.g. R2 damage at red remnant capacity line) and then, at increasing thresholds of exceedance, more severe damage is to be anticipated. For example, at thresholds of 30 and 60 mm exceedance in displacement capacity, shown respectively as green dashed and dotted lines, damage levels R3 and R4 are to be expected.

In other words, the remnant capacity curves can be used to assess the safety margin as well as the anticipated damage level in a rational manner. In burst-prone mines, the displacement and energy criteria must be assessed simultaneously (see Section 6.4.2).

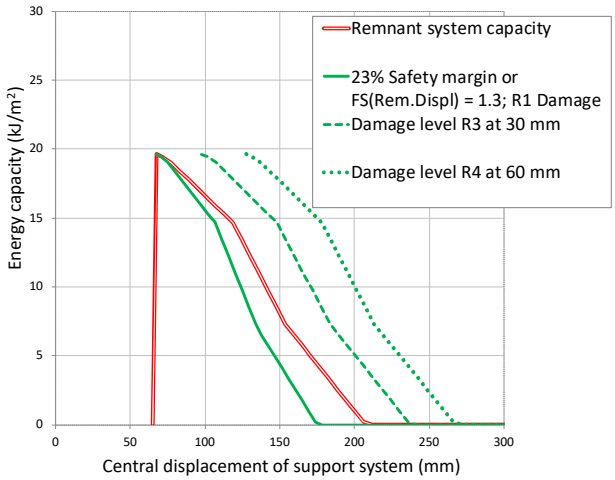


Figure 21 Remnant capacity (red) of the support system used to produce Figure 16b together with three thresholds (green): a displacement-based safety margin (full green line for $FS_{Disp}$ = 1.3), and two potential damage limits R3 and R4 at 30 and 60 mm exceedance (dashed and dotted green lines).

*From common to best practice*

While single pass support systems are cost-efficient, relying on the capacity of the original installed support system can lead to uneconomic and potentially unsafe conditions because mining-induced deformations consume the support capacity. As mining proceeds, both the remnant displacement and energy dissipation capacity, and with it the FS, decrease and the vulnerability of an excavation increases.

When designing a support system best practices consider the potential loss of support capacity over the life of a support system, i.e., the evolution of the demand on the support needs to be defined at the design stage. In otherwise identical ground conditions, support for infrastructures remote from mining, or support in areas affected by extraction, will differ. A proper design focuses on the remnant capacity at the time when loading conditions are most critical, e.g. at the time of dynamic loading by an anticipated seismic event or strainburst.

If support capacity consumption is identified as a critical design criteria the best or most economic practice may involve proactive support maintenance (PSM) based on reliable support performance monitoring (e.g. digital displacement records).

### 6.3 *Mobilizing the self-supporting capacity of a support system*

The most fundamental principle of rock support is to make the reinforced ground self-supporting by creating a stable rock/support arch. This is to be achieved for static or dynamic loading.

For potentially unstable blocks of representative size $B$, Lang (1961) proposed a bolt spacing $s \leq 4B$; e.g. for blocky ground, stress-fractured, or veined rock $s \leq 0.8$ to 2 m. He also suggested a bolt length $L \geq 2s$, i.e. $L = 1$ to 3 m for blocky or fractured rock (Fig. 22a).

In the inner shell (Section 3.2.2), rock fragments may be smaller than the representative block size and a robust retention system has to be selected to prevent unraveling.

#### 6.3.1 *Gabion concept*

For wall support in cave mining, the equivalent model to Lang's self-supporting arch model is to create 'gabions'. Just like for slope stability (Fig. 22b), gabions have to provide:

- immediate retention of broken or fractured rock;
- reinforcement of broken rock in the inner shell;
- surface pressure increasing the self-supporting capacity of broken rock; and
- bulking restraint by reinforcement.

In this manner, a support system is created that behaves like a gabion or an arch (Fig. 22c) and

- provides a radial resistance (orange arrows in Fig. 22d) to the rock mass (e.g. a pillar) behind the gabion; and
- provides tangential resistance (orange arrows in Fig. 22d) to resist the tangential strain driver (HW/FW convergence) causing rock mass bulking.

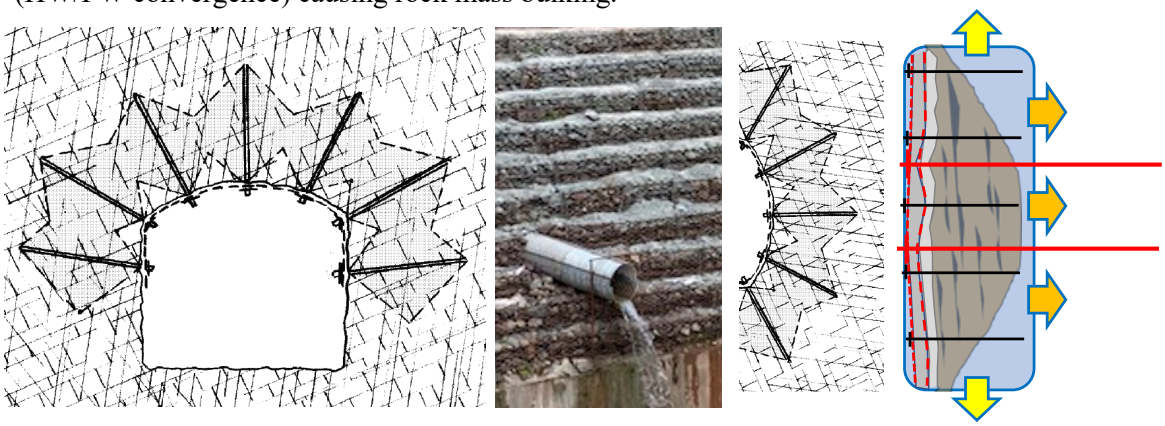

(a) (b) (c) (d)

Figure 22 (a) Supported rock arch principle (Hoek et al. 1995); Gabion concept: (b) support of slope; (c) representation of self-supporting wall rock arch, and (d) flat wall equivalent showing tangential resistance forces (yellow, vertical) and radial confining forces (orange, horizontal).

### 6.3.2 *Why and how gabions work*

The gabion concept works as an integrated support system consisting of a robust surface support system to ensure full utilization of the capacity of the rock mass reinforcement. A gabion ensures that the surface support is not the weakest link. Furthermore, if combined with relatively dense bolting (typically with $s \leq 1$ m), the gabion also facilitates load splitting by direct and indirect loading of the bolts.

The performance of the gabion support, however, depends on whether the loading is

- by tangential straining (e.g. between HW and FW convergence); or
- by radial loading (e.g. by the sudden bulking inside or behind the gabion).

If loaded inside or via straining of the reinforced annulus, all bolts and cables get activated and yield together in direct and indirect loading. However, if a strainburst occurs behind the gabion (typically at > 2 m in mining), the gabion acts as a 'super plate' or a surface support beam, and dissipates energy as it moves into the excavation. In this case, the support elements inside the burst volume (behind the gabion) dissipate energy by indirect loading and the mass of the gabion consumes energy as it is deformed and laterally translated.

As indicated above, effective gabions provide both tangential and radial resistances and when deformed dissipate energy by tangential straining as well as by internal bulking with frictional strength mobilization of the reinforced broken rock. This is illustrated next by using discrete element numerical models (UDEC or 3DEC) to simulate the behavior of a gabion-supported pillar wall.

#### 6.3.2.1 *Tangential load and energy capacity of gabion-supported wall*

Figure 23 presents tangential stress versus tangential strain graphs for two models, one with strong and the other with weak rock blocks (in black: UCS = 60 MPa; $m_i$ =18; $\sigma_t$ = 7 MPa, and in red: UCS = 40 MPa; $m_i$ = 15; $\sigma_t$ = 7 MPa). The discrete element model with Voronoi blocks represents the left wall of a pillar with a zero lateral displacement boundary at the right side of the model. This boundary condition was chosen to approximate conditions of pillars with an elastic core. As a consequence, stress arching occurs, as shown by the stress contours in the insert on the left, and displacements of the stress fractured rock are horizontal (radial) toward the excavation. This leads to the rather ductile response of the pillar wall shown in the graph despite the brittle nature of the simulated fractured rock mass.

The tangential energy dissipation capacity of the reinforced pillar wall is represented by the area under these curves. For a 2.2 m deep gabion of 4.5 m in height, the gabion supported wall in weak rock dissipates 8 kJ/m and in strong rock 14 kJ/m (i.e. per meter along the wall; or 2 to 3 kJ/m$^2$).

The load (and energy) capacity of the pillar wall supported by a 'weak rock' gabion is roughly half of that with a 'strong rock' gabion. Both exhibit a ductile behavior with < 20% strength drop beyond peak. In this model, the support only adds between 10 and 25% to the tangential load bearing capacity of the gabion. Much of the stabilizing force (yellow up and down arrows) comes from the internal resistance of the confined fractured rock inside the gabion and stress arching behind the gabion.

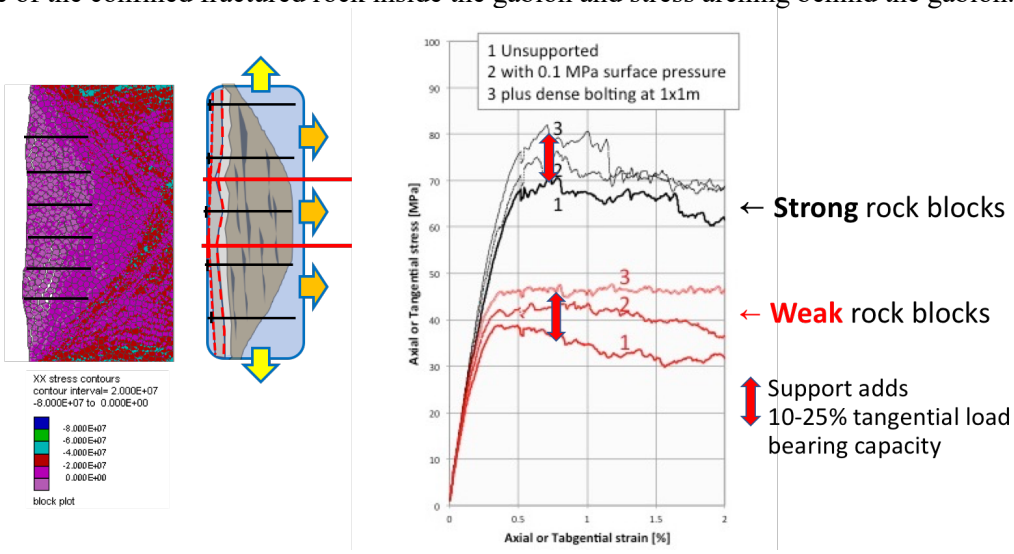


Figure 23 Discrete element modeling results showing the schematic tangential load capacity of a gabion-supported pillar wall with strong (black curves) and weak (red) rock blocks: (1) unreinforced with minor surface

support pressure $p_s$ = 0.01 MPa, (2) with $p_s$ = 0.1 MPa applied at the wall, and (3) same as (2) but with dense bolting at 1 m × 1 m spacing.

#### 6.3.2.2 *Radial support provided by gabions*

For Case (3) in Figure 23 with radial support provided by dense bolting, Figure 24 presents the radial stresses at three locations and for four tangential strain levels of 0.5 to 2%:

- Inside the gabion: the average inter-block pressure increases from 6 to 10 MPa and this provides frictional strength to the gabion as it is strained;
- Immediately behind the gabion (at 2.5 m): the average inter-block pressure first increases to 5 MPa and then drops to about 2.5 MPa at 2% tangential strain providing effective confinement to the pillar; and
- 1 m behind the gabion at 3.5 m from the wall, i.e. at the transition from the inner and outer shell of the pillar, the average radial pressure increases rapidly to 20 MPa due to stress arching.

At first sight, these pressures may seem high. They can be understood when considering the effect of dense bolting within the gabion. Inside the gabion, geometric bulking and block rotation is resisted by the reinforcement. This leads to high inter-block stresses and friction that results in the average pressures shown in Figure 24. The pressures are lower immediately behind the gabion in the unreinforced rock, and they drop to lower values as the gabion is forced to move into the excavation. At 2% tangential strain, approximately 50% of these inter-block pressures are lost behind the gabion but the average 'gabion support' pressure is still superior to the pressure generated by the support components alone.

Beyond the gabion, the horizontal stresses increase rapidly because the rock mass is still cohesive due to the limited damage at the transition to the elastic pillar core. The pressure transmitted by the gabion to the rock mass behind the gabion is at least 10-times higher than the equivalent surface pressure (0.3 MPa resulting from the surface pressure plus distributed bolt loads). The gabion acts like a superplate and transmits the support capacity and the resistance of the confined broken rock to the surrounding rock mass. The gabion therefore greatly enhances the self-supporting capacity of the rock mass in the outer shell. This radial confinement increases the pillar strength. In caving operations, this helps to improve the reliability of a footprint and consequently the reliability of production.

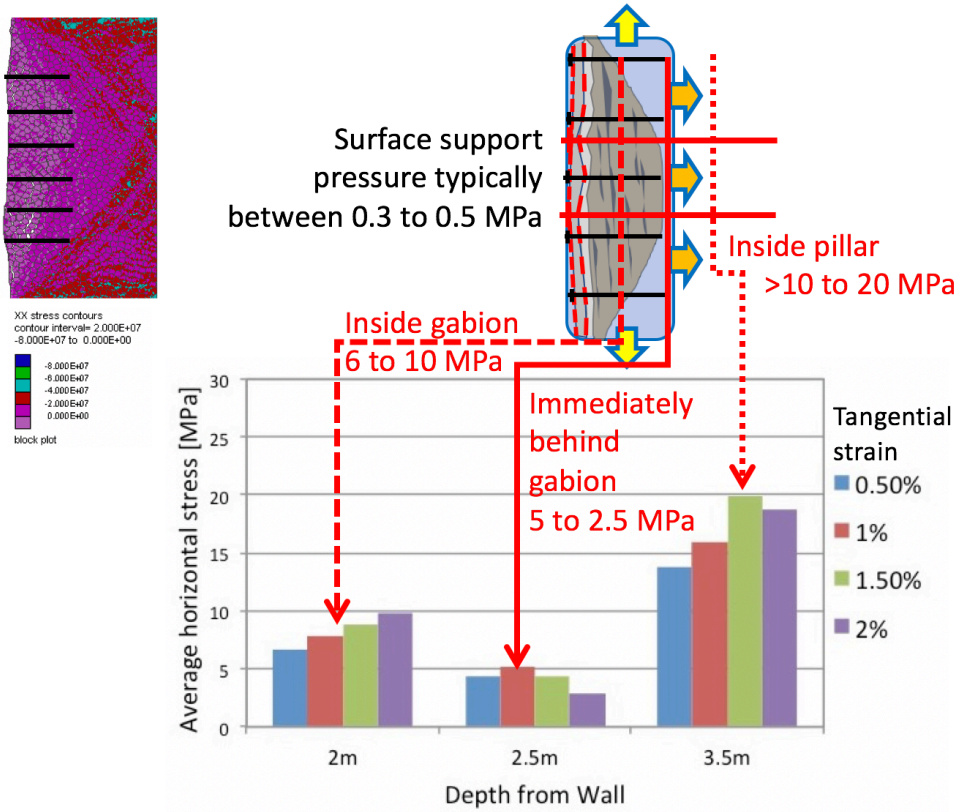


Figure 24 Discrete element modeling results showing the schematic radial pressure capacity of a gabion at increasing tangential strain levels (0.5 to 2%): inside the gabion at 2 m from the wall, immediately behind the gabion at 2.5 m, and 1 m into the pillar at 3.5 m from the wall.

### 6.3.3 *Application of gabion concept from bursting to squeezing ground*

The gabion concept with varying support system components finds applications in a wide spectrum of rock mass behavior; i.e. from bursting to blocky to yielding and even squeezing ground. Figure 25 presents two examples showing a support system consisting of:

a) rockbolts with cable bolts and mesh-reinforced shotcrete: the gabion support successfully prevented damage on the right whereas it collapsed on the left due to excessive bulking during a rockburst; and
b) rockbolts and shotcrete panels with cables and compression slots between the panels: yielding steel sets or shear resistance cable patterns are needed to ensure the overall stability of the schematically illustrated gabion panel system (Fig. 25b).

The gabion concept also finds application in intermediate conditions with blocky and laminated ground.

*From common to best practice*

Common practice of support design without giving due consideration to the self-stabilizing action of well-constrained broken rock is flawed. The integrated support capacity of a gabion is far superior to the capacity of the support components alone. It provides a most effective support system to resist static and dynamic load demands by creating self-supporting rock arches.

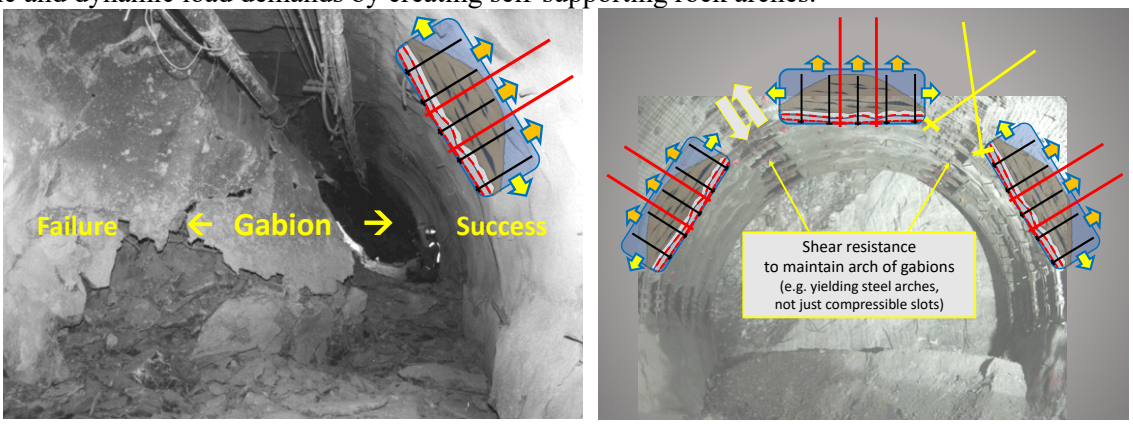


(a) (b)

Figure 25 Gabion concept application for the entire spectrum from (a) bursting to blocky to deformable to (b) squeezing ground.

### 6.4 *Deformation-based support selection for stress-fractured rock*

In stress-fractured ground, two mechanisms affect the excavation performance during construction: (1) raveling of broken rock resulting in short stand-up times, and (b) large deformations caused by geometric bulking imposing large radial deformations on the support. The first is met by ensuring robust rock retention and the second by providing a deformable bolting system.

The challenge of controlling highly stressed brittle rock in civil and mining projects with deformation compatible support was addressed by the author in the written version of the Sir Allan Muir Wood lecture entitled “Ground Support for Constructability of Deep Underground Excavations” (Kaiser 2016). For detailed discussions of the support selection process, the reader is also referred to Kaiser (2014).

A deformation-based support design to manage bulking aims at two fundamental support design axioms:

- Control of the cause for bulking by minimizing the tangential straining of the rock in the immediate vicinity of an excavation (resist HW/FW closure as illustrated by the yellow arrows in Fig. 22d and 23); and
- Control of the geometric bulking of stress-fractured ground by rock reinforcement inside the gabion and the application of confining pressure by the gabion to the surrounding ground (Fig. 22d).

Because the product of the displacement times resisting force represents the energy dissipated by the supported rock ( $E \sim F^{*}\delta$ ), a deformation-based design implicitly deals with energy dissipation by the integrated support system, and therefore is applicable to conditions where the rock fails in a violent

manner during a rockburst. For both static and dynamic loading, the displacement demand has to be estimated (Section 6.4.2).

### 6.4.1 *How do bolts work – how do they get loaded?*

Before the demand can be estimated, it is necessary to understand 'How bolts work?' Do they carry a load at the plate, or do they reinforce the rock mass to create a self-supporting rock arch. In other words, do they dissipate energy in direct, indirect, or combined loading?

For static mining-induced loading, Figure 26 presents the load distribution along un-plated cable bolts (bar graphs provide bolt load) and the yield (red) and failure locations (black). In two of the four locations highlighted by the red ellipses, tensile yield led to failure (lower two ellipses) whereas in the upper two ellipses, shear contributed to the failure. It follows that both internal axial and shear demands need to be defined. Most importantly, this simulation illustrates that bolts get indirectly loaded and eventually fail internal to the deforming rock mass.

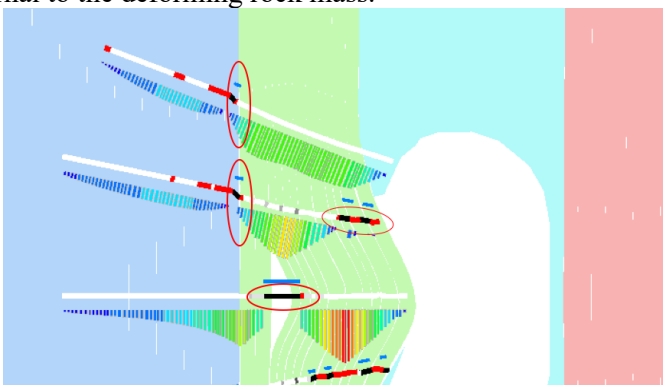

Figure 26 Simulation of cable bolt loading during vertical/tangential straining of laminated rock (Itasca 3DEC simulation; Pierce 2017; pers. com.). Color scheme: Bolts – red = yield, black = failed in tension or shear; bar charts: bolt load from cold to warm. Displacement scale exaggerated.

For support in burstprone ground, it is frequently assumed that bolts get loaded via the plate and that the capacity obtained from pullout tests is representative. This is rarely the case because the rock mass fractures and bulks inside the burst volume. This is illustrated by the horizontal displacement profile for three simulated time steps in Figure 27a after a strainburst was initiated at about 2 m from the wall (Gao et al. 2019). The horizontal displacement at the wall is about half of the displacement inside the rock mass.

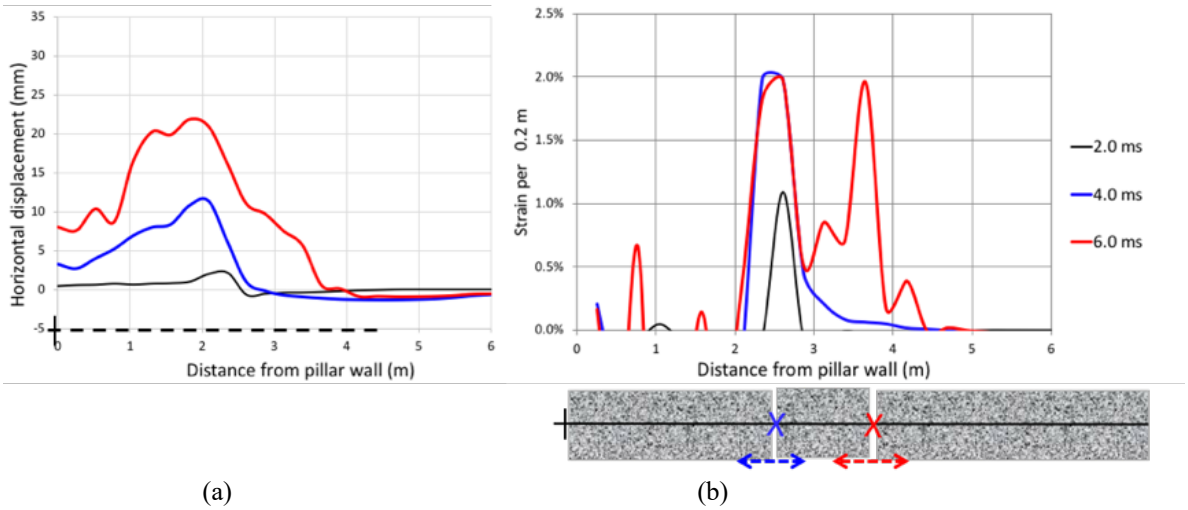


(a) (b)

Figure 27 (a) Simulated horizontal displacement and (b) relative displacement (strain) induced by strainbursts (modified after Gao et al. 2019).

The corresponding relative displacement or strain over a yield length of 0.2 m is shown in Figure 27b. Extension strain peaks (positive) are first observed at 2.3 m (at 4 ms) and then at 3.6 m (at 6 ms) from the wall. At the same time, a compressive strain peak is encountered at 1.1m depth. A bolt crossing this strain profile will be strained in compression at 1.1 m due to compression of the previously fractured (spalled) ground. This reverses static extension straining in the first 1 to 2 m from the wall and unloads the bolt. A bolt will therefore fail at deeper seated locations with elevated extension strain and not necessarily at or near the plate. Interestingly, while wall displacements do occur, the steel near the plate experiences much less strain at this stage in the loading process. A radially installed bolt therefore gets indirectly loaded and dissipates energy inside the rock mass.

Clearly, the displacement demand and its distribution along the bolts need to be understood and quantified to select appropriate support components for an integrated support system.

### 6.4.2 *Static and dynamic support system demand estimation*

For support design purposes, it is necessary to estimate the displacement and energy demands such that they can be compared with the remnant support system capacity (Section 6.2.6). The displacement demand is obtained from the bulking of the spalling or strainbursting ground (Section 3.2.4). The energy demand for strainbursts is composed of two energy sources, the energy transmitted by a stress wave from a remote seismic source and the energy release at the strainburst location.

#### 6.4.2.1 *Displacement demand*

The displacement demand for continuum behavior can be estimated from analytical or numerical models. However, for brittle rock with geometric bulking most models are deficient and tend to underestimate bulking displacements. For brittle rock, the semi-empirical approach outlined in Section 3.2.4 (as well as by Kaiser 2016c; Kaiser and Cai (2019)) can be adopted whereby the depth of failure (Eqns 8 and 9) or the depth of strainbursting is combined with representative bulking factors (Fig.12) to quantify the internal strain and the cumulative displacement over the length of a bolt.

#### 6.4.2.2 *Energy demand*

*Energy from triggered strainbursts*

As discussed in Section 2.3.2, the bulking velocity $v_B$ at the inner edge of the burst volume depends on the time it takes to fail the burst volume ($t_R$). This rupture time varies widely depending on the brittleness of the rock. It typically ranges from 1/10 to 1/20 of a second (or less in extreme conditions) and controls the bulking velocity. For example, for 1 m of strainbursting ground with $BF$ = 5% the burden ahead of the burst volume is suddenly displaced by 50 mm, resulting in a bulking velocity $v_B$ between 0.5 and 1 m/s (2.5 m/s for $t_R$ = 1/50 s). If 1 m$^3$ of spalled rock (burden) is moved at this velocity, the kinetic energy $E_B = ½\ m\ v_B^2$ ranges from 0.3 to 1.3 kJ/m$^2$ (8.1 kJ/m$^2$ for $t_R$ = 1/50 s). This simple example demonstrates that the available kinetic energy is highly sensitive to the rupture time and that high velocities can be attributed to self-initiated or triggered strainbursts.

*Energy from dynamically-loaded strainbursts*

If combined with a large remote seismic event, the ground motion $PGV$ at the strainburst location can be obtained from applicable ground motion prediction equations (GMPE). Then, the dynamic stresses can be calculated to estimate the incremental deepening of the failure zone and the associated incremental bulking displacement (Kaiser et al. (1996), Kaiser and Cai (2019). Furthermore, the ground motion from the remote seismic event increases the velocity of the burden and possibly also ejects part of the burst volume. The kinetic energy demand therefore is obtained from the combined velocity.

The results of a displacement and energy demand analysis is graphically presented in the displacement versus energy graphs of Figure 28 together with an example of a remnant support system capacity (red line). For a range of variable parameters and for a seismic event of magnitude $M_L$ = 0 to 4 at a distance of $R$ = 30 m, the red path (full line) represents the demand for a scenario where the burden is 'ejected'. The black dashed path is for 'ejection' of the burden and the entire strainburst volume.

For this example, it is assumed that the central deflection before the burst was 62 mm. A pure strainburst adds 62 mm for a total displacement demand of 124 mm. The energy demand ranges from 0.5 to 1.0 kJ/m$^2$ for the two mass assumptions (Points A and A'). With the remote seismic event of magnitude $M_L$ = 3, the displacement is increased by 14 mmm to 138 mm due to the deepening of the fracture zone and the energy is augmented by the ground motions to 3.7 and 9.1 kJ/m$^2$ (Points B & B').

The capacity for FS = 1.3 is again shown in green. In this example, the demands do not reach the remnant support system capacity at $M_L$ = 3. If only the burden is 'ejected' (Points B), the FS >1.5 and if the burden and the strainburst volume is 'ejected FS < 1.3 (Point B'). The minimum factor of safety at Point B' in terms of displacements $FS_{Disp}$ = 143/138 = 1.04 and in terms of energy $FS_{Energy}$ = 10.6 /9.1 = 1.16. This is far from the commonly but incorrectly estimated $FS_{Energy}$ = remnant capacity before the burst (30 kJ/m$^2$) / energy demand (9.1 kJ/m$^2$) = 3.3 for this case.

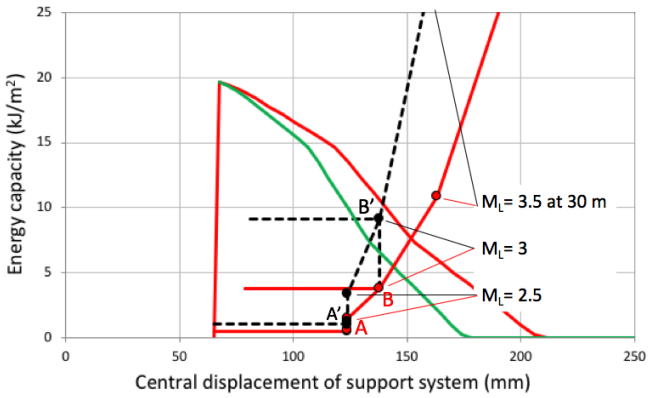


Figure 28 Comparison of displacement and energy demand estimates with simulated support system capacity (red; FS = 1.3 in green): for strainburst at *SL* = 0.8 and when combined with a remote seismic event for $M_L$ = 0 to 4 at R = 30 m.

The path in Figure 28 shows that a strainburst primarily shifts the displacement demand to the right consuming much displacement capacity, and the remote seismic event moves the energy demand up although only for $M_L$ > 2. This is consistent with findings of Morissette et al. (2012) , who found that remote seismic events tend to aggravate the damage when the event magnitude exceed 1.5 to 2 (Cai & Kaiser 2018).

This example further amplifies the need for a deformation-based support design, particularly when dynamic perturbations impose an energy demand.

*From common to best practice*

Again, ample opportunities and economic as well as safety benefits can be derived by moving from common support selection to deformation-based support system design practices. Common practices of support design without giving due consideration to the displacement demand are flawed and common practice of pure energy-based design for burstprone ground is highly flawed. Both can lead to serious safety hazards.

Deformation-based support selection constitutes best practice for ground control in highly stressed, brittle failing ground. In burstprone ground, the displacement and energy demand from strainbursts and from remote seismic events must be simultaneously considered. It is essential to compare the demands to the remnant capacity and not to the capacity of the originally installed support system.

## 7 CONCLUSION – MOVE TO BEST PRACTICES !

Common practices are often not best practices when judged from an economic or workplace safety perspective, and common practices that worked well at shallow depth may need to be replaced because the rock mass behavior has changed and poses new hazards at depth.

This lecture focused specifically on opportunities resulting from better means to assess the vulnerability of excavations, to characterize the rock mass, for ground control, and rockburst damage mitigation. It is demonstrated that ample opportunities exist to derive benefits from moving from common to best practices. In summary, opportunities are identified in the following areas:

- Identification of engineering design parameters EDPs that characterize the vulnerability and fragility of underground excavations.
- Rock mass characterization that follows a systematic process of moving from inferred to proven rock mass quality designations.
- Grouping of rock mass qualities into three classes (RMQ1 to 3) that reflect three characteristic rock mass and excavation behavior modes.

- Methods to obtain appropriate rock and rock mass strength envelopes for peak, post-peak and residual strength.
- Practices that respect the limitations of classification and characterization systems, in particular, in the use of GSI-strength equations for rock mass strength determination for good rock.
- Differentiation between near wall (inner and outer shell) behaviors for support design and pillar sizing.
- Deformation-based support selection for ground control in highly stressed, brittle failing ground.
- Utilization of the self-stabilizing capacity of well-constrained broken rock by adopting the gabion concept to provide effective support to resist static and dynamic load demands.
- Quantification of support capacity consumption as a critical design criteria.
- Use of proactive support maintenance (PSM) based on support deformation monitoring to restore consumed support capacity.
- Consideration of the impact of pre-burst support deformation and bulking displacements resulting from strainbursts.
- Replacement of energy-based by displacement-based support designs for burst-prone ground.

Best practices take, at the design stage, the evolution of deformation demands over the life of an excavation into account. Proper designs focuses on the remnant support capacity at the time when loading conditions are most critical.

We cannot stagnate and accept the status quo. We have to implement the advanced state-of-the-art by adopting best practices that respect the actual behavior of the rock, excavations and support. Those that 'hide behind' standard or common practice might be liable when others have adopted better or best practices.

## ACKNOWLEDGEMENTS

The authors wish to acknowledge the many contributions of industrial sponsors, Rio Tinto through the Rio Tinto Centre for Underground Mine Construction, Freeport McMoran, LKAB, Vale, Glencore, as well as the financial contributions of NSERC (Natural Sciences and Engineering Research Council of Canada).

Much of the presented material is a result of long-term collaborations and the efforts of graduate students. The list of individuals who have contributed in some form to the research reflected in this article is too long, but the author wishes to collectively recognize that much value was derived from their discussions and contributions. The author thanks them all in this anonymous fashion – you know who you are.

Nevertheless, I like to specifically acknowledge a few individuals who have certainly influenced the findings, lessons learned and conclusions presented in this lecture. In alphabetic order, they are Drs. F. Amann, N. Bahrani, R. Bewick, M. Cai, M. Diederichs, E. Eberhardt, H-B. Kim, D. Martin, D. McCreath and M. Pierce.

## REFERENCES

*Books*

Cai, M. & Kaiser, P.K. 2018. Rockburst phenomena and support characteristics, Volume I in Rockburst Support Reference Book. MIRARCO Laurentian University, preliminary ISBN: 978-0-88667-096-2, 191 p. (released May 2018).

Kaiser, P.K. & Cai, M. 2019. Rock support to mitigate rockburst damage caused by dynamic excavation failure, Volume II in Rockburst Support Reference Book. MIRARCO Laurentian University, preliminary ISBN: 978-0-88667-097-9 (to be released late 2019).

Kaiser, P.K. 2017. Excavation vulnerability and selection of effective rock support to mitigate rockburst damage. In X.-T. Feng (Ed.), Rockburst: mechanisms, monitoring, warning, and mitigation. New York: Elsevier. ISBN: 978-0-12-805054-5, 473–518.

Kaiser, P.K., McCreath, D.R. & Tannant, D.D. 1996. Rockburst Support. In Canadian Rockburst Research Program 1990-95. Vol.2, 324 p. (Published by CAMIRO, Sudbury).

Hoek, E., Kaiser, P.K. & Bawden, W.F. 1995. Rock Support for Underground Excavations in Hard Rock. A.A. Balkema, Rotterdam, 215 p.

Hutchinson, D.J. & Diederichs, M.S. 1996. Cablebolting in Underground Hard Rock Mines, Bitech Publishers Ltd., Richmond, BC, Canada, 406 p.

Müller, L. 1963. Der Felsbau. F. Enke Verlag, Stuttgart, Vol.1, 624 p.

*Articles*

Bahrani, N. & Kaiser, P.K. 2016. Strength degradation approach (SDA) for estimation of confined strength of micro-defected Rocks. ARMA 16-890

Bahrani N., Kaiser, P.K. 2013. Strength degradation of non-persistently jointed rock mass. Technical note: *International Journal of Rock Mechanics & Mining Sciences*, 62:28–33.

Barton, N. & Grimstad, E. 1994. The Q-system following twenty years of application in NMT support selection. 43rd Geomechanics Colloquy. Felsbau, 6/94: 428-436.

Barton, N., Bandis, S. & Bakhtar, K. 1985. Strength, deformation and conductivity coupling of rock joints. *Int. J. of Rock Mechanics & Mining Sciences*, 22(3): 121-140.

Bewick, R.P., Kaiser, P.K. & Amann, F. 2019. Strength of massive to moderately jointed hard rock masses. Rock Mechanics and Geotechnical Engineering, 11(3): 562-575 https://doi.org/10.1016/j.jrmge.2018.10.003

Bewick, R. P., Amann, F., Kaiser, P.K. & Martin, C.D. 2015. Interpretation of UCS test results for engineering design. 13th ISRM International Congress of Rock Mechanics, Montreal, Canada, 14 p.

Bieniawski, Z. T. 1979. Tunnel design by rock mass classifications. U.S. Army Waterways Experiment Stgation, Technical Report No. GL-79-19, 131 p..

Bieniawski, Z. T. 1976. Rock mass classification in rock engineering. In: Proc. Symp. on Exploration for Rock Engineering, Z.T. Bieniawski (editors), Cape Town. 1: 97-106.

Brown, E.T. 2007. Block caving geomechanics. University of Queensland, Second edition, 696 p.

Garza-Cruz, T.V., Pierce, M. & Kaiser, P.K. 2015. Use of 3DEC to study spalling and deformation associated with tunneling at depth. DeepMining'14, ACG (eds. Hudyma and Potvin), 13 p.

Gao, F., Kaiser, P.K., Stead, D., Eberhardt, E. & Elmoe, D. 2019. Strainburst phenomena and numerical simulation of self-initiated brittle rock failure. International Journal of Rock Mechanics and Mining Sciences, 116: 52-63.

Gao, F., Kaiser, P.K., Stead, D., Eberhardt, E. & Elmo, D. 2019. Numerical simulation of strainbursts using a novel initiation method. Computers and Geotechnics, 106: 117-127.

Diederichs, M. S. 2007. Mechanistic interpretation and practical application of damage and spalling prediction criteria for deep tunneling (2003 Canadian geotechnical Colloquium), Canadian Geotechnical Journal, 44(9): 1082–1116. DOI: 10.1139/T07–033.

Hoek, E. & Brown, E.T. 2019. The Hoek-Brown failure criterion and GSI -218 edition. Journal of Rock Mechanics and Geotechnical Engineering, 11(3): 445-463.

Hoek, E., Kaiser, P.K. & Bawden, W.F. 1995. Rock Support for Underground Excavations in Hard Rock. A.A. Balkema, Rotterdam, 215 p.

Kaiser, P.K. 2017. Ground control in strainbursting ground - A critical review and path forward on design principles. 9TH Int. Symp. on Rockbursts and Seismicity in Mines, Santiago, Chile, 146-158.

Kaiser, P.K. 2016a. Challenges in rock mass strength determination for design of deep underground excavations. ISRM on-line lecture (45 min) https://www.isrm.net/gca/?id=1227

Kaiser, P.K. 2016b. Underground rock engineering to match the rock's behaviour - a fresh look at old problems. MTS lecture at 50th US Rock Mechanics Symp., 6., abridged summary in ISRM news 2017.

Kaiser, P.K. 2016c. Ground Support for Constructability of Deep Underground Excavations - Challenge of managing highly stressed brittle rock in civil and mining projects. ITA Sir Muir Wood lecture of Intern. Tunneling Association at World Tunneling Congress, San Francisco, 33 p. www.ita-aites.org or http://www.mirarco.org/grc/#ert_pane1-4

Kaiser, P.K. 2014. Deformation-based support selection for tunnels in strain-burstprone ground. DeepMining'14, ACG (eds. Hudyma and Potvin), 227-240.

Kaiser P.K. 2006. Rock mechanics considerations for construction of deep tunnels in brittle rock. Asia Rock Mechanics Symposium, Singapore, 12 p.

Kaiser P. K., F. Amann & Bewick, R.P. 2015. Overcoming Challenges of Rock mass Characterization for Underground Construction in Deep Mines. 13th ISRM Intern. Congress of Rock Mechanics, 10-13 May, Montreal, Canada, 14 p.

Kaiser, P.K. & Cai, M. 2013. Critical review of design principles for rock support in burst-prone ground – time to rethink! Ground Support 2013, Potvin, Y. and Brady, B. (eds), Perth, Australia, 3-38.

Kaiser, P.K., Diederichs, P.K., Martin, C.D., Sharp, J. & Steiner W. 2000. Underground works in hard rock tunneling and mining. GeoEng 2000, Melbourne, Australia, Technomic Publ. Co., 1: 841-926.

Kaiser, P.K. & Kim, B-H. 2014. Characterization of strength of intact brittle rock considering confinement dependent failure processes. Rock Mech Rock Eng.; DOI 10.1007/s00603-014-0545-5.

Kaiser, P.K & Kim, B-H. 2008. Rock mechanics advances of underground construction and mining. Korea Rock Mechanics Symposium, Seoul, 1-16.

Kaiser, P.K., Maloney, S. & Yong, S. 2016. Role of large scale heterogeneities on in-situ stress and induced stress fields. ARMA 16-571.

Lang, T.A. 1961. Theory and practice of rockbolting. Trans. Amer. Inst. Min. Engrs, 220: 333-348.
Martin, C.D. 2019. Stress-induced fracturing (Spalling) around underground excavations: Laboratory and in-situ observations. ISRM on-line lecture, https://www.isrm.net/gca/?id=1359
Martin, C.D. 1997. The effect of cohesion loss and stress path on brittle rock strength. Canadian Geotechnical Journal, **34**(5): 698-725.
Martin, C.D., Kaiser, P.K. & Christiansson, R. 2003. Stress, instability and design of underground excavations. International Journal of Rock Mechanics and Mining Sciences, 40(7-8): 1027-1047.
Morissette, P., Hadjigeorgiou, J., Thibodeau, D. & Potvin, Y. 2012. Validating a support performance database based on passive monitoring data. 6th Int. Seminar on Deep and High Stress Mining, 41-55.
Ortlepp, W.D. 2005. A review of the contribution to the understanding and control of mine rockbursts 6th Int. Symp. on Rockbursts and Seismicity in Mines, ACG, Y. Potvin, M. Hudyma (Eds.), Perth, Australia, 3-20.
Perras, M.A. & Diederichs, M.S. 2016. Predicting excavation damage zone depths in brittle rocks. J. of Rock Mechanics and Geotechnical Engng, 8(1): 60-74.
Potvin, Y. 2009. Strategies and tactics to control seismic risks in mines. J. South Afr. Inst. Min. Metall., 109: 177-186.
Schofield, A.N. 1998 (and 2001) The "Mohr-Coulomb" Error. CUED/D-SOILS/TR305; presented in Paris at jubilee of Pierre Habib; published in "Mechanique et Geotechnique", Balkema, 6 p.
Tarasov, B.G. & Potvin, Y. 2012. Absolute, relative and intrinsic rock brittleness at compression. Mining Technology 121(4): 218-225.
Terzaghi, K. 1946. Rock defects and loads on tunnel supports. In Rock tunneling with steel supports, (eds R. V. Proctor and T. L. White) 1, Youngstown, Commercial Shearing and Stamping Company, 17-99.
Wawersik, W.R. & Fairhurst, C. 1970. A study of brittle rock fracture in laboratory compression experiments. Int. J. of Rock Mechanics and Mining Sciences, 7(5): 561–575.